Available online at www.sciencedirect.com
ScienceDirect
Journal of Sound and Vibration 308 (2007) 348–372
JOURNAL OF SOUND AND VIBRATION
www.elsevier.com/locate/jsvi

Short Communication

Direct identification and expansion of damping matrix for experimental–analytical hybrid modeling

Gokhan O. Ozgen, Jay H. Kim*

Structural Dynamics Research Lab, Mechanical, Industrial and Nuclear Engineering Department, University of Cincinnati, Cincinnati, OH 45221-0072, USA

Received 27 January 2006; received in revised form 11 September 2006; accepted 26 July 2007
Available online 4 September 2007

Abstract

The theory of direct experimental identification of damping matrix based on the dynamic stiffness matrix (DSM) method is further developed in this work. Based on the relationship between the DSMs of the smaller experimental model and larger analytical model, the mathematical relationship between the damping matrices of the two models is established. Examining the relationship, two methods are developed that can be used to expand the experimental damping matrix to the size of the analytical model. Validity of the expansion methods is demonstrated with numerical examples. The expanded damping matrix is intended to be combined with analytically formulated stiffness and mass matrices to build an experimental–analytical hybrid model. To find the frequency range, in which such a hybrid modeling is valid, a simple but effective method is developed.

1. Introduction

A damping model should represent both the mechanism and spatial distribution of the energy loss in the system. In contrast to the mass and stiffness matrices, formulation of the damping matrix still stands as a big challenge in modeling a linear dynamic system. Commonly used simple models such as the proportional damping or structural damping model are used for no reason but mathematical convenience. Various models such as viscoelastic [1,2], friction [3], micro-slip [4], and air damping [5,6] have been used to describe damping mechanism, while much less efforts have been made to represent the spatial distribution of damping.

Motivated by the desire for accurate simulation of dynamic systems, a substantial amount of research effort has been made to develop experimental damping identification methods. In those methods a proportional or structural damping matrix is frequently used, which is not finding but assuming the forms for the mechanism and the spatial distribution of damping. Furthermore, the damping matrix is formulated often by utilizing modal parameters such as natural frequencies, natural modes, and modal damping ratios extracted from measured frequency response functions (FRFs) [7–17]. There are some methods developed to obtain the damping matrix directly from measured FRFs, thus eliminating the need to identify modal parameters [18–22].

*Corresponding author. Tel.: +1 513 556 6300.
E-mail address: jay.kim@uc.edu (J.H. Kim).

0022-460X/$ - see front matter © 2007 Elsevier Ltd. All rights reserved.
doi:10.1016/j.jsv.2007.07.044

Nomenclature

$\mathbf{A}_{\omega_1}$	coefficient matrix
c	viscous damping coefficient
$\mathbf{C}$	viscous damping matrix
$\mathbf{C}_i$	ith coefficient matrix
dof	degree of freedom
DSM	dynamic stiffness matrix
$\mathbf{D}$	structural damping matrix
$f_i(\omega)$	ith frequency function
FRF	frequency response function
$\mathbf{F}(\omega)$	harmonic force vector
$\mathbf{H}(\omega)$	FRF matrix
$\mathbf{H}_{\text{exp}}(\omega)$	experimental FRF matrix
$\mathbf{H}_h(\omega)$	FRF matrix of the hybrid model
$\mathbf{I}$	identity matrix
j	complex term $(=\sqrt{-1})$
k	number of frequency points/stiffness
k_i	stiffness of ith element
$\mathbf{K}$	stiffness matrix
$\mathbf{K}_{R\text{mm}}(\omega)$	stiffness matrix of the experimental model
$\mathbf{L}(\omega)$	generalized damping matrix
$\mathbf{L}_h(\omega)$	expanded damping matrix
$\mathbf{L}_{R\text{mm}}(\omega)$	damping matrix of the experimental model
m	subscript for measured degrees of freedom
m_i	mass of ith element
M	number of measurement points
$\mathbf{M}$	mass matrix
$\mathbf{M}_{R\text{mm}}(\omega)$	mass matrix of the experimental model
N	number of degrees of freedom of the analytical model
$\mathbf{R}_{\text{um}}(\omega)$	transformation matrix
S	number of frequency functions
$\mathbf{S}_D(\omega)$	DSM of analytical model
$\mathbf{S}_{D_R}(\omega)$	experimental DSM
$\mathbf{T}(\omega)$	transformation matrix
$\tilde{\mathbf{T}}(\omega)$	real-valued approximate transformation matrix
u	subscript for unmeasured degrees of freedom
u_n	nth function
$\mathbf{X}(\omega)$	harmonic response vector
$\boldsymbol{\varepsilon}(\omega)$	error matrix
$\boldsymbol{\varepsilon}_p(\omega)$	percent error matrix is
ω	circular frequency (rad/s)
$\mathbf{1}_i$	vector with all components as zero but the component at ith row

The damping identification method developed by Lee and Kim [23] which identifies damping matrices directly from measured frequency response functions is unique as it formulates the damping matrix from the dynamic stiffness matrix (DSM). The DSM is obtained by inverting the measured FRF matrix, which is utilizing the fact that the imaginary part of the DSM is the damping matrix.

The DSM-based direct damping identification method is very attractive because it can be applied to any linear dynamic systems and does not use any arbitrary assumptions. However two fundamental issues were encountered while implementing the method [24–26], which are the difficulty of expanding the identified matrix to the size of the analytical model of the system and the high sensitivity of the accuracy of the result to measurement errors. While these issues are being addressed in our ongoing research, this paper deals with the first one, expansion of the identified damping matrix to the size of the analytical model. Major outcomes of the study presented in this paper are: (1) explicit relationship between the smaller, identified damping matrix and the larger damping matrix of the analytical model, (2) error analysis to understand the limitation of the DSM-based damping identification method, and (3) the method to expand the experimentally formulated damping matrix to the size of the analytical model to formulate the hybrid system equation.

2. Theoretical development

2.1. Dynamic stiffness matrix-based damping matrix identification [23]

Direct damping identification method developed by Lee and Kim [23] can be summarized in three steps. In the first step, measured frequency response functions are put into a square matrix form

as follows:

$$\mathbf{H}_{\text{exp}}(\omega) = \begin{bmatrix} H_{11}(\omega) & H_{21}(\omega) & \cdots & H_{1M}(\omega) \\ H_{12}(\omega) & H_{22}(\omega) & \cdots & \vdots \\ \vdots & \vdots & \ddots & \vdots \\ H_{M1}(\omega) & \cdots & \cdots & H_{MM}(\omega) \end{bmatrix}, \tag{1}$$

where $\mathbf{H}_{\text{exp}}(\omega)$ is the experimental frequency response function matrix, ω is the circular frequency (rad/s) and M is the number of measurement points. In the second step, the dynamic stiffness matrix $\mathbf{S}_{D_{\text{exp}}}(\omega)$ defined at the experimental degrees of freedom (dofs) is computed by inverting $\mathbf{H}_{\text{exp}}(\omega)$; i.e.

$$\mathbf{S}_{D_{\text{exp}}}(\omega) = \mathbf{H}_{\text{exp}}(\omega)^{-1}. \tag{2}$$

The final step utilizes the fact that the real part of the dynamic stiffness matrix $\mathbf{S}_{D_{\text{exp}}}(\omega)$ represents the mass and stiffness properties and the imaginary part represents the loss property, i.e.; $\mathbf{S}_{D_{\text{exp}}}(\omega) = -\omega^2\mathbf{M}_{\text{exp}} + \text{j}\mathbf{L}_{\text{exp}}(\omega) + \mathbf{K}_{\text{exp}}$, where $\mathbf{M}_{\text{exp}}$ is the mass matrix, $\mathbf{K}_{\text{exp}}$ is the stiffness matrix of the experimental model, and $\text{j} = \sqrt{-1}$. $\mathbf{L}_{\text{exp}}(\omega)$, a generalized damping matrix, can be obtained as

$$\mathbf{L}_{\text{exp}}(\omega) = \text{Imag}\left(\mathbf{S}_{D_{\text{exp}}}(\omega)\right), \tag{3}$$

where $\mathbf{L}_{\text{exp}}(\omega)$ becomes a matrix of general function of frequency. The frequency distribution at each matrix element represents the damping mechanism at the corresponding nodal point and relative magnitudes of the elements at the given frequency point represent the spatial distribution of damping. The viscous and structural damping matrices $\mathbf{C}_{\text{exp}}$ and $\mathbf{D}_{\text{exp}}$ are special cases that can be found by the linear regression of the measured frequency response functions as follows:

$$\begin{bmatrix} \mathbf{D}_{\text{exp}} \\ \mathbf{C}_{\text{exp}} \end{bmatrix}_{2M\times M} = \begin{bmatrix} \mathbf{I} & \omega_1\mathbf{I} \\ \mathbf{I} & \omega_2\mathbf{I} \\ \cdot & \cdot \\ \cdot & \cdot \\ \mathbf{I} & \omega_k\mathbf{I} \end{bmatrix}^{+}_{kM\times 2M} \begin{bmatrix} \text{Imag}\left[\mathbf{H}_{\text{exp}}(\omega_1)^{-1}\right] \\ \text{Imag}\left[\mathbf{H}_{\text{exp}}(\omega_2)^{-1}\right] \\ \cdot \\ \cdot \\ \text{Imag}\left[\mathbf{H}_{\text{exp}}(\omega_k)^{-1}\right] \end{bmatrix}_{kM\times M}, \tag{4}$$

where "+" represents the pseudo-inverse of the matrix, $\mathbf{I}$ is the identity matrix, and k is the number of frequency points of the frequency response function data used in the regression. The set of matrices $\mathbf{C}_{\text{exp}}$ and $\mathbf{D}_{\text{exp}}$ found as such will be the best representation of the damping by a linear function of the frequency.

While the identification procedure provides a damping matrix of the size of experimental degrees of freedom, we often need a matrix of much larger size. Building an experimental-FEM hybrid model by combining an experimentally identified damping matrix and theoretically formulated mass and stiffness matrices is a good example. In order to expand the damping matrix obtained from the DSM-based approach, the relationship between the damping matrices of different sizes of the same system should be derived. To achieve this objective, first the dynamic stiffness matrix of the large size analytical model and the dynamic stiffness matrix of the smaller size experimental model is related in Section 2.2. Then finally, an explicit relationship between the damping matrices of the larger, analytical model and the smaller experimental model is derived in Section 2.4.

2.2. Relating experimental and analytical models

Both the analytical and experimental models approximate the original continuous system of infinite degrees of freedom by finite number of dofs as illustrated in Fig. 1. Usually the number of dofs of the experimental model is much smaller than that of the analytical model. We consider that the analytical model has N degrees of freedom, and M of those are measured degrees of freedom of the experimental model.

In the analytical model of N degrees of freedom, harmonic input–output relationship between the response $\mathbf{X}(\omega)$ and the force $\mathbf{F}(\omega)$ is

$$\mathbf{S}_D(\omega)\mathbf{X}(\omega) = \mathbf{F}(\omega), \tag{5}$$

where $\mathbf{S}_D(\omega)$ is the dynamic stiffness matrix of size $N \times N$, which is defined as

$$\mathbf{S}_D(\omega) = -\omega^2\mathbf{M} + \mathrm{j}\mathbf{L}(\omega) + \mathbf{K}. \tag{6}$$

The response and force vectors can be arranged by partitioning measured and unmeasured groups of degrees of freedom:

$$\mathbf{X}(\omega) = \begin{Bmatrix} \mathbf{X}_m(\omega) \\ \mathbf{X}_u(\omega) \end{Bmatrix}, \tag{7}$$

$$\mathbf{F}(\omega) = \begin{Bmatrix} \mathbf{F}_m(\omega) \\ \mathbf{F}_u(\omega) \end{Bmatrix}, \tag{8}$$

where subscripts m and u in Eqs. (7) and (8) stand for the measured and unmeasured parts.

The harmonic input–output relationship of the analytical model can also be written using the FRF matrix as follows:

$$\mathbf{X}(\omega) = \mathbf{H}(\omega)\mathbf{F}(\omega). \tag{9}$$

When partitioned into measured and unmeasured components, Eq. (9) becomes

$$\begin{Bmatrix} \mathbf{X}_m(\omega) \\ \mathbf{X}_u(\omega) \end{Bmatrix} = \begin{bmatrix} \mathbf{H}_{\mathrm{mm}}(\omega) & \mathbf{H}_{\mathrm{mu}}(\omega) \\ \mathbf{H}_{\mathrm{um}}(\omega) & \mathbf{H}_{\mathrm{uu}}(\omega) \end{bmatrix} \begin{Bmatrix} \mathbf{F}_m(\omega) \\ \mathbf{F}_u(\omega) \end{Bmatrix}, \tag{10}$$

where $\mathbf{H}_{\mathrm{mm}}(\omega)$ is the measured frequency response function matrix.

In a typical modal test, the structure is excited only at measurement points, thus $\mathbf{F}_u(\omega) = \mathbf{0}$. The harmonic input–output relation of the full-size analytical model that describes the experiment becomes

$$\begin{Bmatrix} \mathbf{X}_m(\omega) \\ \mathbf{X}_u(\omega) \end{Bmatrix} = \begin{bmatrix} \mathbf{H}_{\mathrm{mm}}(\omega) & \mathbf{H}_{\mathrm{mu}}(\omega) \\ \mathbf{H}_{\mathrm{um}}(\omega) & \mathbf{H}_{\mathrm{uu}}(\omega) \end{bmatrix} \begin{Bmatrix} \mathbf{F}_m(\omega) \\ \mathbf{0} \end{Bmatrix}. \tag{11}$$

Substituting $\mathbf{F}_u(\omega) = \mathbf{0}$ into Eq. (5), the DSM relationship can also be rewritten in the same manner:

$$\begin{bmatrix} \mathbf{S}_{D\mathrm{mm}}(\omega) & \mathbf{S}_{D\mathrm{mu}}(\omega) \\ \mathbf{S}_{D\mathrm{um}}(\omega) & \mathbf{S}_{D\mathrm{uu}}(\omega) \end{bmatrix} \begin{Bmatrix} \mathbf{X}_m(\omega) \\ \mathbf{X}_u(\omega) \end{Bmatrix} = \begin{Bmatrix} \mathbf{F}_m(\omega) \\ \mathbf{0} \end{Bmatrix}. \tag{12}$$

On the other hand, the DSM relationship of the experimental model is

$$\mathbf{S}_{D_R}(\omega)\mathbf{X}_m(\omega) = \mathbf{F}_m(\omega), \tag{13}$$

where $\mathbf{S}_{D_R}(\omega)$ stands for the dynamic stiffness matrix of the experimental model. The subscript "R" is used replacing the subscript "exp" used earlier for Eq. (2), because the experimental model is essentially a

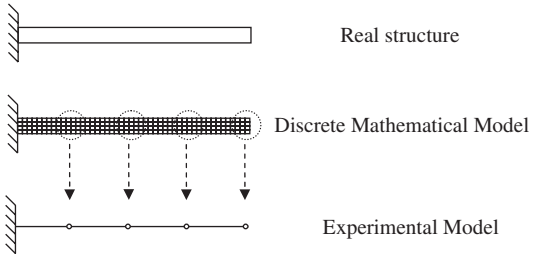

Fig. 1. Models of different number of degrees of freedom for the same structure.

"reduced" version of the analytical model. As defined in Eq. (2), the experimental dynamic stiffness matrix is the inverse of the measured frequency response function matrix, i.e. $\mathbf{S}_{D_R}(\omega) = \mathbf{H}_{\mathrm{mm}}(\omega)^{-1}$.

Eq. (12) can be rewritten as

$$\mathbf{S}_{D\mathrm{mm}}(\omega)\mathbf{X}_m(\omega) + \mathbf{S}_{D\mathrm{mu}}(\omega)\mathbf{X}_u(\omega) = \mathbf{F}_m(\omega), \tag{14}$$

$$\mathbf{S}_{D\mathrm{um}}(\omega)\mathbf{X}_m(\omega) + \mathbf{S}_{D\mathrm{uu}}(\omega)\mathbf{X}_u(\omega) = \mathbf{0}. \tag{15}$$

From Eq. (15):

$$\mathbf{X}_u(\omega) = -\mathbf{S}_{D\mathrm{uu}}(\omega)^{-1}\mathbf{S}_{D\mathrm{um}}(\omega)\mathbf{X}_m(\omega). \tag{16}$$

Substituting Eq. (16) into Eq. (14), the following equation is obtained:

$$\left(\mathbf{S}_{D\mathrm{mm}}(\omega) - \mathbf{S}_{D\mathrm{mu}}(\omega)\mathbf{S}_{D\mathrm{uu}}(\omega)^{-1}\mathbf{S}_{D\mathrm{um}}(\omega)\right)\mathbf{X}_m(\omega) = \mathbf{F}_m(\omega). \tag{17}$$

Comparing Eqs. (17) and (13), we realize:

$$\mathbf{S}_{D_R}(\omega) = \mathbf{S}_{D\mathrm{mm}}(\omega) - \mathbf{S}_{D\mathrm{mu}}(\omega)\mathbf{S}_{D\mathrm{uu}}(\omega)^{-1}\mathbf{S}_{D\mathrm{um}}(\omega). \tag{18}$$

Eq. (18) relates $\mathbf{S}_{D_R}(\omega)$, dynamic stiffness matrix of the experimental model, and $\mathbf{S}_D(\omega)$, dynamic stiffness matrix of the analytical model. Because our interest is on the relationship between damping matrices, we try to derive an explicit relationship between the damping matrices, i.e., imaginary parts of these two DSMs.

The dynamic stiffness matrix of the experimental model $\mathbf{S}_{D_R}(\omega)$can be written as

$$\mathbf{S}_{D_R}(\omega) = -\omega^2\mathbf{M}_{R\mathrm{mm}}(\omega) + j\mathbf{L}_{R\mathrm{mm}}(\omega) + \mathbf{K}_{R\mathrm{mm}}(\omega), \tag{19}$$

where $\mathbf{M}_{R\mathrm{mm}}(\omega)$, $\mathbf{L}_{R\mathrm{mm}}(\omega)$ and $\mathbf{K}_{R\mathrm{mm}}(\omega)$ are the mass, damping and stiffness matrices of the reduced-size experimental model. In the appendix, it is shown that these matrices are related with those of the analytical model as follows:

$$\mathbf{M}_{R\mathrm{mm}}(\omega) = \mathbf{T}(\omega)^{\mathrm{T}}\mathbf{M}\mathbf{T}(\omega), \tag{20}$$

$$\mathbf{L}_{R\mathrm{mm}}(\omega) = \mathbf{T}(\omega)^{\mathrm{T}}\mathbf{L}(\omega)\mathbf{T}(\omega), \tag{21}$$

$$\mathbf{K}_{R\mathrm{mm}}(\omega) = \mathbf{T}(\omega)^{\mathrm{T}}\mathbf{K}\mathbf{T}(\omega). \tag{22}$$

The transformation matrix $\mathbf{T}(\omega)$ relates the measured portion of the response vector to the full-size response vector, i.e., $\mathbf{X}(\omega) = \mathbf{T}(\omega)\mathbf{X}_m(\omega)$. We note:

$$\mathbf{T}(\omega) = \begin{bmatrix} \mathbf{I} \\ -\mathbf{S}_{D\mathrm{uu}}(\omega)^{-1}\mathbf{S}_{D\mathrm{um}}(\omega) \end{bmatrix}. \tag{23}$$

From Eq. (21), the damping matrix of the reduced-size experimental model can be found from the damping matrix of the full-size analytical model; however, what we need is the other way, finding the latter from the former. That procedure will be developed in later discussions.

The process to represent a larger model using a subset of the degrees of freedom, in our case the experimental model, is often called "dynamic condensation" in literature. The formulation of the reduced dynamic stiffness matrix given in Eq. (19) is common to most condensation methods available. Some of these methods formulate an equivalent dynamic transformation matrix defined similar to Eq. (23). System Equivalent Reduction Expansion Process (SEREP) [27] and Improved Reduced System (IRS) [28] are examples to these kinds of methods. Reviews of this group of methods can be found in Refs. [29,30]. Another group of methods uses an iterative approach to obtain the equivalent dynamic transformation matrix. A review of iterative condensation methods can be found in Ref. [31]. In both approaches, the main objective is to obtain a dynamic transformation matrix that will result in a DSM of the reduced model which can produce accurate modal parameters of the structure of interest. Among the iterative methods, the one developed by Paz [32] derives the dynamic transformation matrix in the exact same form of Eq. (23). However, Paz's method [32] uses an iterative procedure to come up with the frequency value that will result in an optimum equivalent transformation matrix [30], while in our study the dynamic transformation matrix is kept

frequency dependent. The dynamic transformation matrix as defined in Eq. (23) represents an exact, frequency-by-frequency condensation of the DSM of the original degrees of freedom to a reduced size.

Before proceeding further, we discuss frequency dependency of the matrices of the experimental model utilizing the relationships shown in Eqs. (20)–(22).

2.3. Frequency dependency of system matrices of the experimental model

Examining the system matrices of the experimental model defined in Eqs. (20)–(22), it is seen that they are not constant but functions of frequency because the transformation matrix $\mathbf{T}(\omega)$ is a function of frequency.

This effect can be demonstrated using a numerical example. Suppose that a 4 degrees of freedom model is described by a 2 degrees of freedom experimental model as shown in Fig. 2. The situation can be interpreted as that we obtain a 2 degrees of freedom experimental model by measuring the 2nd and 4th degrees of freedom of a structure originally represented by a 4 degrees of freedom analytical model. Stiffness and mass values are $k_1 = 2.5 \times 10^5\,\mathrm{N/m}$, $k_2 = 3.5 \times 10^5\,\mathrm{N/m}$, $k_3 = 2.0 \times 10^5\,\mathrm{N/m}$, $k_4 = 3.0 \times 10^5\,\mathrm{N/m}$, $m_1 = 1.3\,\mathrm{kg}$, $m_2 = 3.1\,\mathrm{kg}$, $m_3 = 1.3\,\mathrm{kg}$ and $m_4 = 2.0\,\mathrm{kg}$.The damping matrix is defined as $\mathbf{C} = 5.0 \times 10^{-5} \cdot \mathbf{K}$.

Diagonal elements of the system matrices of the experimental model, $\mathbf{M}_{R\mathrm{mm}}(\omega)$, $\mathbf{L}_{R\mathrm{mm}}(\omega)$ and $\mathbf{K}_{R\mathrm{mm}}(\omega)$, are plotted in Figs. 3a–c in the frequency range that includes all four modes of the analytical model. In the low-frequency range, these plots show that mass and stiffness parameters are constant and damping parameters are linear functions of frequency as expected. All parameters however, become very large around 98.7 Hz and 108 Hz. The plot of two elements of the transformation matrix $\mathbf{T}(\omega)$ in Fig. 4 shows two peaks at the same frequencies too. This observation explains the somewhat unexpected frequency dependency of the elements of the system matrices of the experimental model around 98.7 and 108 Hz. Noting that the term $-\mathbf{S}_{D\mathrm{uu}}(\omega)^{-1}$ is included in the transformation matrix $\mathbf{T}(\omega)$ in Eq. (23), these frequencies are recognized as the eigenvalues of $\mathbf{S}_{D\mathrm{uu}}(\omega)$, the unmeasured part of the dynamic stiffness matrix of the analytical model.

The alternative expression for the experimental dynamic stiffness matrix in Eq. (18), also contains the term $\mathbf{S}_{D\mathrm{uu}}(\omega)^{-1}$ which means that the peak effect will occur on the overall value of the experimental dynamic stiffness matrix too. Note that a typical dynamic stiffness matrix has the form $\mathbf{L}(\omega) = \mathbf{C}_1 + \omega\mathbf{C}_2 + \omega^2\mathbf{C}_3$. Because $\mathbf{M}$, $\mathbf{K}$ $\mathbf{C}$ in this case are constant matrices, real and imaginary parts of the elements of the DSM should normally appear as quadratic and linear functions of frequency, respectively. Figs. 5 and 6 are the spatial plots of the real and imaginary parts of the DSM of the 4 degrees of freedom original model, which clearly show the expected patterns of the typical dynamic stiffness matrix. On the other hand, real and imaginary parts of the experimental dynamic stiffness matrix $\mathbf{S}_{D_R}(\omega)$ plotted in Figs. 7 and 8 show the expected frequency dependency only in the low-frequency range, however followed by sharp peaks and anti-peaks in the high frequency similar to the case of the system matrices (Fig. 3). This observation indicates that the experimental model behaves like a typical dynamic stiffness matrix, or in other words can be represented by constant valued system matrices, only in the low-frequency range which falls to the left of the observed peaks. As we have already discussed, this frequency range is dictated by the eigenvalues of $\mathbf{S}_{D\mathrm{uu}}(\omega)$. Around and beyond this particular frequency limit, it becomes impossible to represent the reduced experimental model with system matrices that physically make sense.

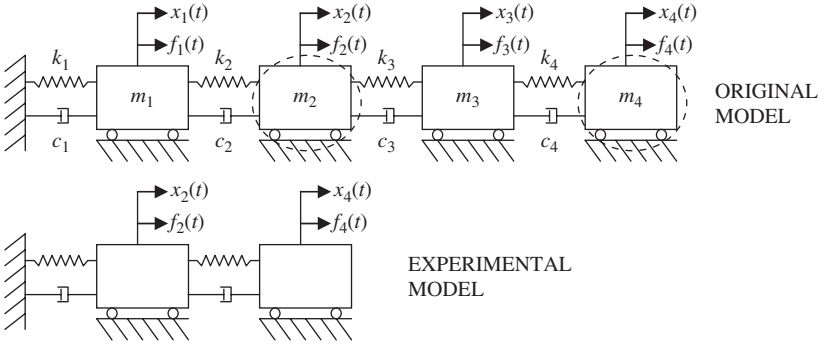

Fig. 2. Numerical example: 4 degrees of freedom lumped parameter original model and 2 degrees of freedom experimental model.

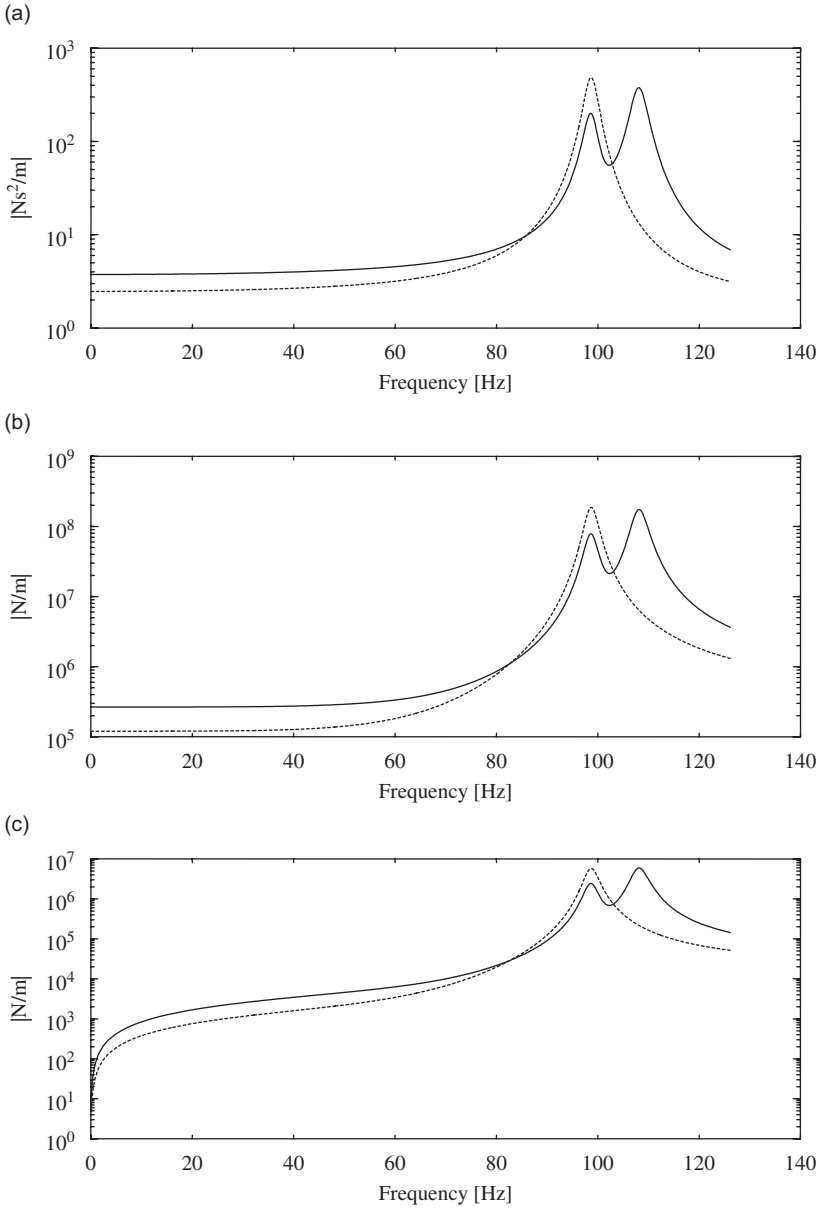

Fig. 3. Magnitudes of the diagonal elements of the system matrices of the experimental model: ——, 2nd dof; ------, 4th dof; (a) Experimental mass matrix $\mathbf{M}_{R_{\mathrm{mm}}}(\omega)$, (b) experimental stiffness matrix $\mathbf{K}_{R_{\mathrm{mm}}}(\omega)$, (c) experimental damping matrix $\mathbf{L}_{R_{\mathrm{mm}}}(\omega)$.

This frequency dependency issue of the system matrices of the experimental model is essentially a manifestation of the fact that the size of the experimental model is insufficient for distinct spatial representation of the mode shapes whose frequencies are close to or higher than the limiting frequency, the lowest eigenvalue of $\mathbf{S}_{D_{\mathrm{uu}}}(\omega)$.

It should be noted that increasing the number of measured degrees of freedom increases the magnitude of the lowest eigenvalue of $\mathbf{S}_{D_{\mathrm{uu}}}(\omega)$. This makes sense since increasing the size of the experimental model increases the chances of accurate representation of higher frequency mode shapes otherwise problematic, which also means that the limiting frequency must also be increased.

This type of frequency limitation of reduced dynamic models imposed by the nature of the dynamic condensation is also discussed by Berman [33–35]. Berman recognizes the frequency dependency of system matrices of reduced models and recommends that it should be properly taken into account when using the dynamic stiffness

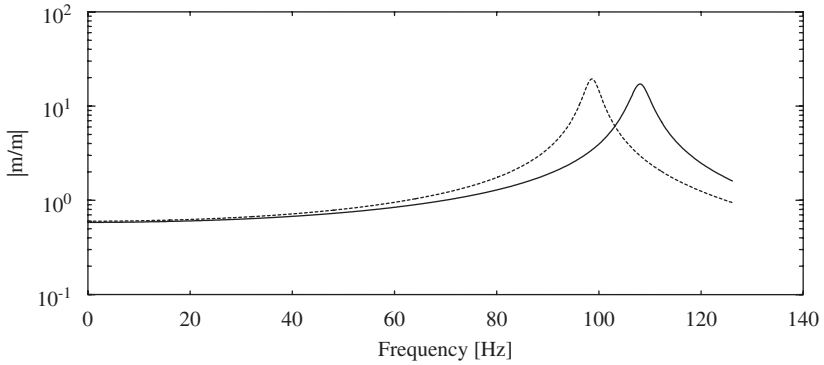

Fig. 4. Magnitudes of two sample elements of the transformation matrix $\mathbf{T}(\omega)$: ——, element located at 3rd row and 1st column; ------, element located at 4th row and 2nd column.

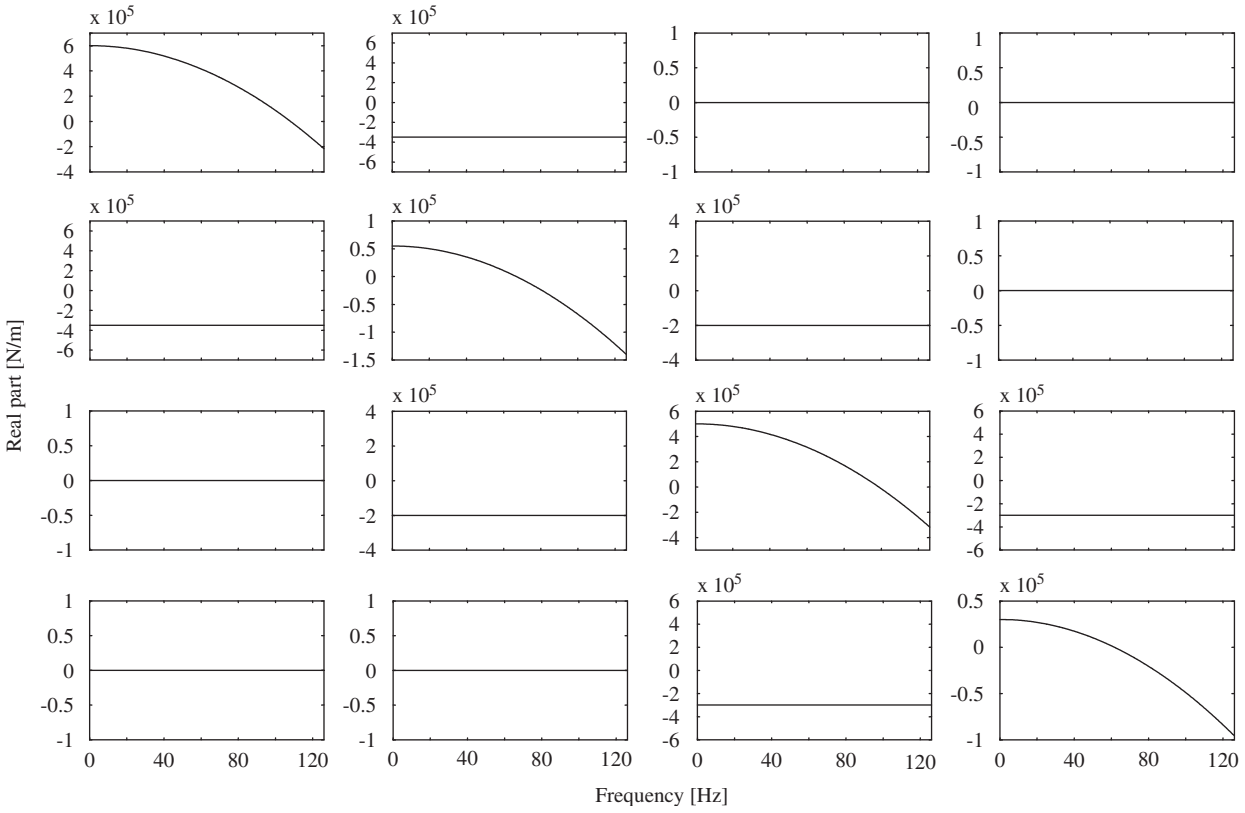

Fig. 5. Spatial plot of the real part of the dynamic stiffness matrix for the 4 degrees of freedom original model.

matrix of the reduced model. In another study by Lammens et al. [36], the limitation caused by the lowest eigenvalue of $\mathbf{S}_{D_{\mathrm{uu}}}(\omega)$becomes a challenge during the implementation of an FRF-based model updating procedure. In this procedure, the error minimization scheme developed for updating the larger size FEA model uses the dynamic stiffness matrix of the experimental model. They encounter the same problem of having sharp peaks at the elements of the experimental dynamic stiffness matrix, and identify this peak frequency as the lowest eigenvalue of $\mathbf{S}_{D_{\mathrm{uu}}}(\omega)$. Recognizing this as a limitation, they recommend using frequencies lower than the first eigenvalue of $\mathbf{S}_{D_{\mathrm{uu}}}(\omega)$. A similar challenge is encountered in the case of optimum selection of measurement degrees of freedom for experimental modal analysis purposes. The main objective in such a study is to select the measurement dofs such that the mode shapes of interest can be distinctly identified. The method developed by

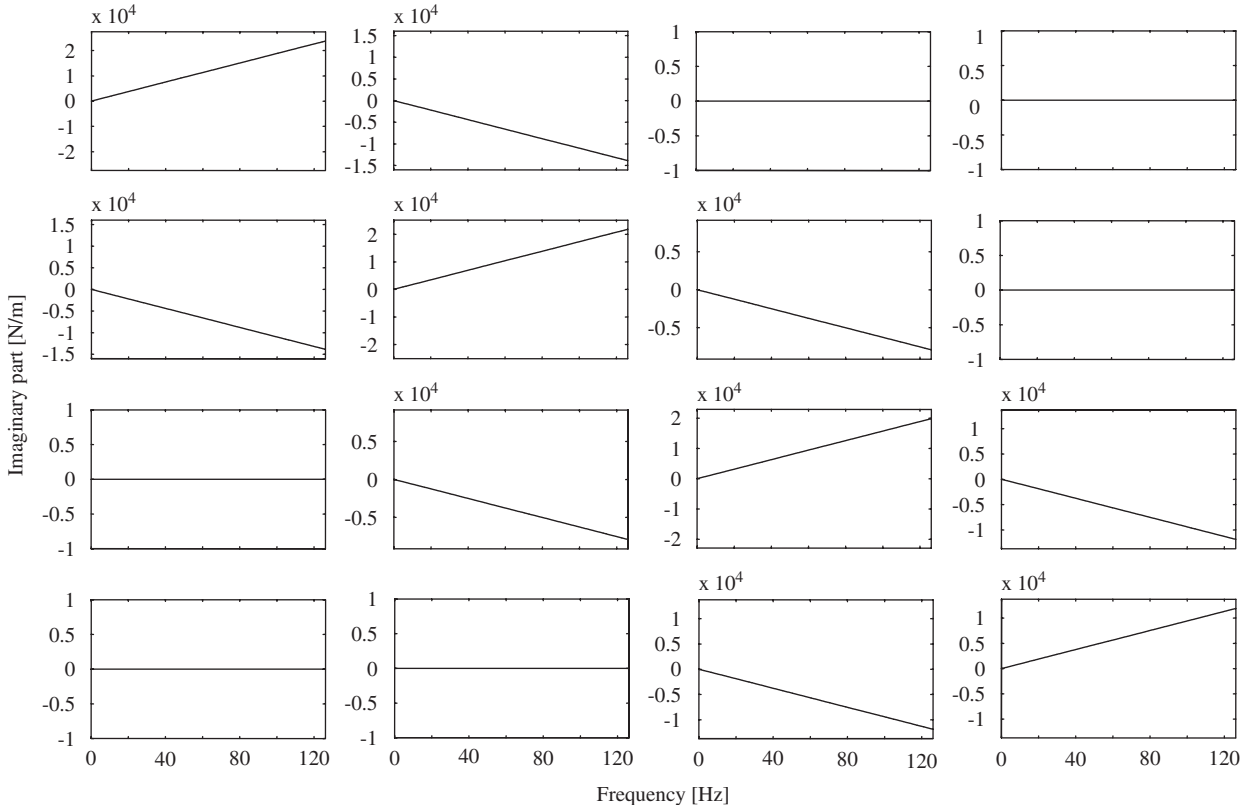

Fig. 6. Spatial plot of the imaginary part of the dynamic stiffness matrix for the 4 degrees of freedom original model.

Bouhaddi et al. [37] uses the dynamic condensation theory to obtain the limiting frequency of the experimental model as the smallest eigenvalue of $\mathbf{S}_{D_{uu}}(\omega)$. It then uses this criterion for optimum selection of experimental dofs. The selection of degrees of freedom is done iteratively with the objective of maximizing the limiting frequency.

The eigenvalues of the dynamic stiffness matrix component $\mathbf{S}_{D_{uu}}(\omega)$ can actually be located by applying the singular value decomposition to the measured frequency response function matrix $\mathbf{H}_{mm}(\omega)$. When singular values of the measured frequency response function matrix $\mathbf{H}_{mm}(\omega)$ are plotted as functions of frequency, antiresonances observed in the plots occur at the eigenvalues of $\mathbf{S}_{D_{uu}}(\omega)$. Singular value plots of the measured frequency response function matrix of the 2 degrees of freedom experimental model are shown in Fig. 9, which shows two antiresonances that exactly match with the two eigenvalues of the $\mathbf{S}_{D_{uu}}(\omega)$. This is an important observation because it indicates that the frequency range, in which the experimental model is valid, can be directly found from the singular value plots of the measured frequency response function matrix $\mathbf{H}_{mm}(\omega)$ rather than by numerically computing the eigenvalues of $\mathbf{S}_{D_{uu}}(\omega)$.

Note that as seen in Fig. 10, which plots singular values of the FRF matrix of the original 4 degrees of freedom model, singular value plots of the full-size FRF matrix $\mathbf{H}(\omega)$ do not contain any antiresonances. It should also be noted that antiresonance points in the FRFs of the original model and antiresonance points in the singular value plots of the measured frequency response function matrix $\mathbf{H}_{mm}(\omega)$, do not have any correlations. This can be easily seen from the plots of the frequency response functions of the original 4 degrees of freedom model (Fig. 11), whose antiresonance points are different from the antiresonances of the same system's $\mathbf{H}_{mm}(\omega)$ singular value plots (97 and 108 Hz).

2.4. Relating damping matrices of the experimental and analytical models

In addition to the relationship between damping matrices of the experimental and analytical models established in Eq. (21), there are two more important issues that have to be addressed.

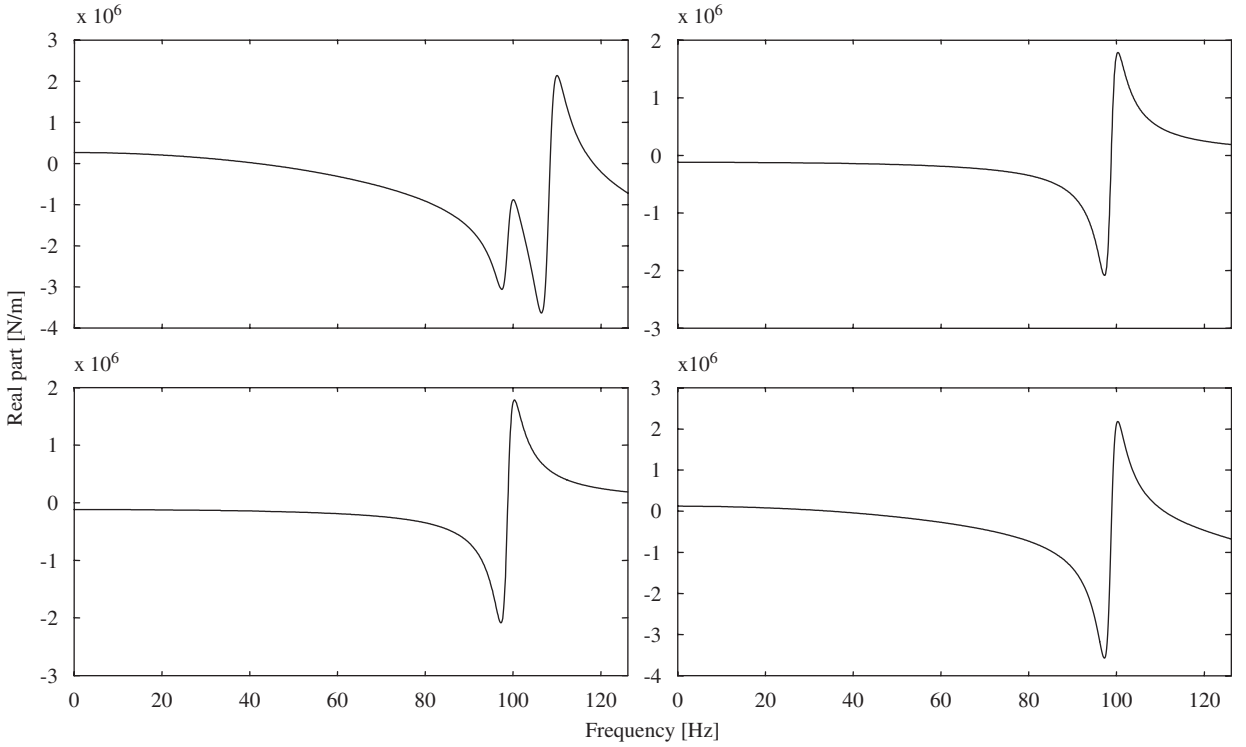

Fig. 7. Spatial plot of the real part of the dynamic stiffness matrix for the 2 degrees of freedom experimental model.

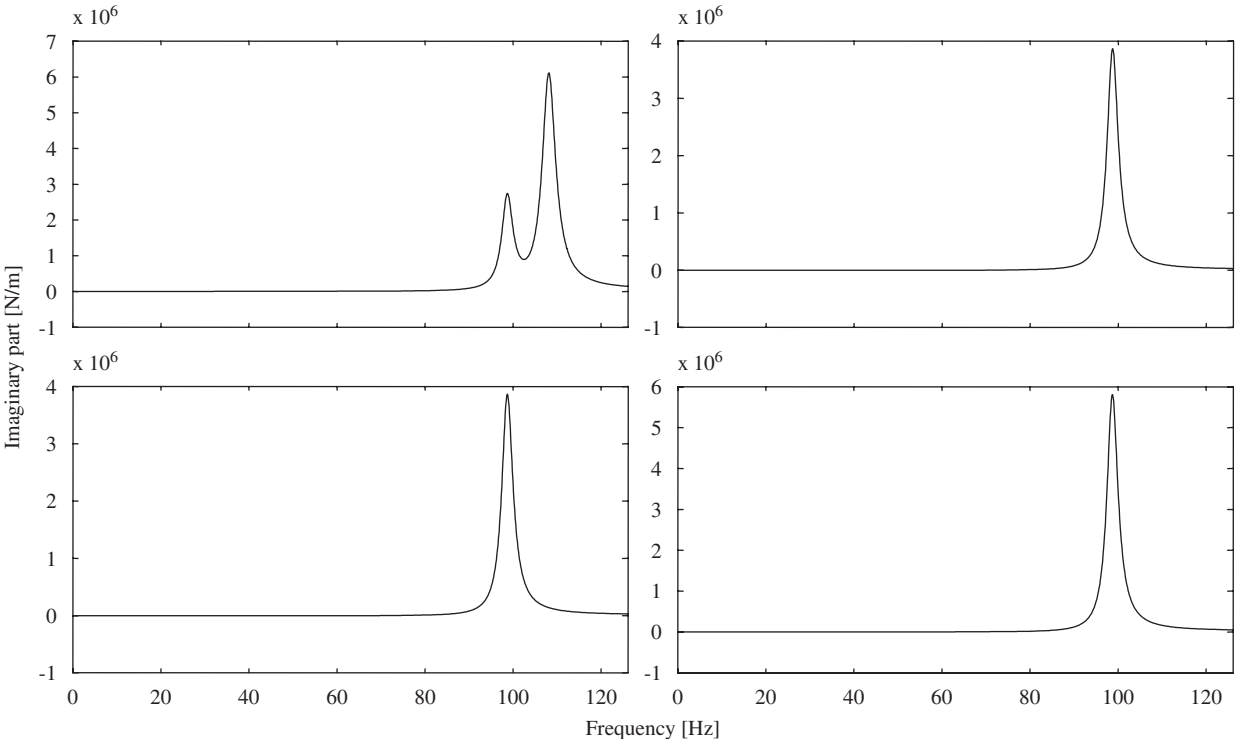

Fig. 8. Spatial plot of the imaginary part of the dynamic stiffness matrix for the 2 degrees of freedom experimental model.

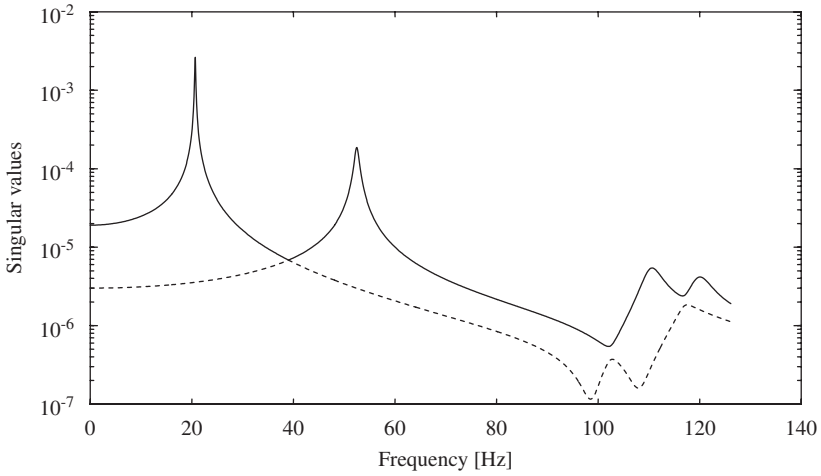

Fig. 9. Singular value plots of the frequency response function matrix for the 2 degrees of freedom experimental model: ——, largest singular value; ------, second largest singular value (or lowest).

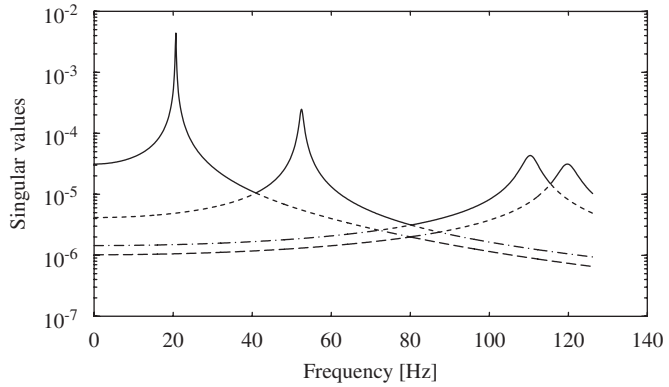

Fig. 10. Singular value plots of the frequency response function matrix for the 4 degrees of freedom original model; ——, largest singular value: ------, second largest singular value; –·–·–, third largest singular value; ––––, fourth largest singular value (or lowest).

First, $\mathbf{L}_{R_{\mathrm{mm}}}(\omega)$ is not the entirety of the imaginary part of the experimental dynamic stiffness matrix because $\mathbf{T}(\omega)$ is complex valued. By the same reason, $\mathbf{M}_{R_{\mathrm{mm}}}(\omega)$ and $\mathbf{K}_{R_{\mathrm{mm}}}(\omega)$ are also not real, but complex valued. Therefore,

$$\mathrm{Imag}\big(\mathbf{S}_{D_R}(\omega)\big) = \mathrm{Imag}\big(\mathrm{j}\mathbf{L}_{R_{\mathrm{mm}}}(\omega)\big) + \mathrm{Imag}\big(-\omega^2\mathbf{M}_{R_{\mathrm{mm}}}(\omega)\big) + \mathrm{Imag}\big(\mathbf{K}_{R_{\mathrm{mm}}}(\omega)\big). \tag{24}$$

Consequently, $\mathbf{L}_{R_{\mathrm{mm}}}(\omega)$ will approximate the damping matrix, only if the imaginary part of $\mathbf{T}(\omega)$ is small compared to its real part, i.e.

$$\mathbf{L}_{R_{\mathrm{mm}}}(\omega) \approx \mathrm{Imag}(\mathbf{S}_{D_R}(\omega)). \tag{25}$$

The plots in Fig. 12 are the real and imaginary parts of one of the elements of the transformation matrix $\mathbf{T}(\omega)$ that relates the 2 degrees of freedom and 4 degrees of freedom models shown in Fig. 2. It is seen that the imaginary component becomes large around 97 Hz, which is the lowest eigenvalue of $\mathbf{S}_{D_{\mathrm{uu}}}(\omega)$. Fig. 13 shows the same information as Fig. 12, but in terms of the percent ratio of the imaginary part to the real part. In the low-frequency range of 0–70 Hz, the imaginary part is smaller than 1% of the real part, meaning $\mathbf{L}_{R_{\mathrm{mm}}}(\omega)$ accurately represents the damping effect of the experimental model.

Second, the transformation matrix $\mathbf{T}(\omega)$ contains the unmeasured parts of the dynamic stiffness matrix, $\big(-\mathbf{S}_{D_{\mathrm{uu}}}(\omega)^{-1}\mathbf{S}_{D_{\mathrm{um}}}(\omega)\big)$, which is not completely available as the analytical model only provides the mass and stiffness terms of the unmeasured part of the system, but not the damping terms. However, in the frequency

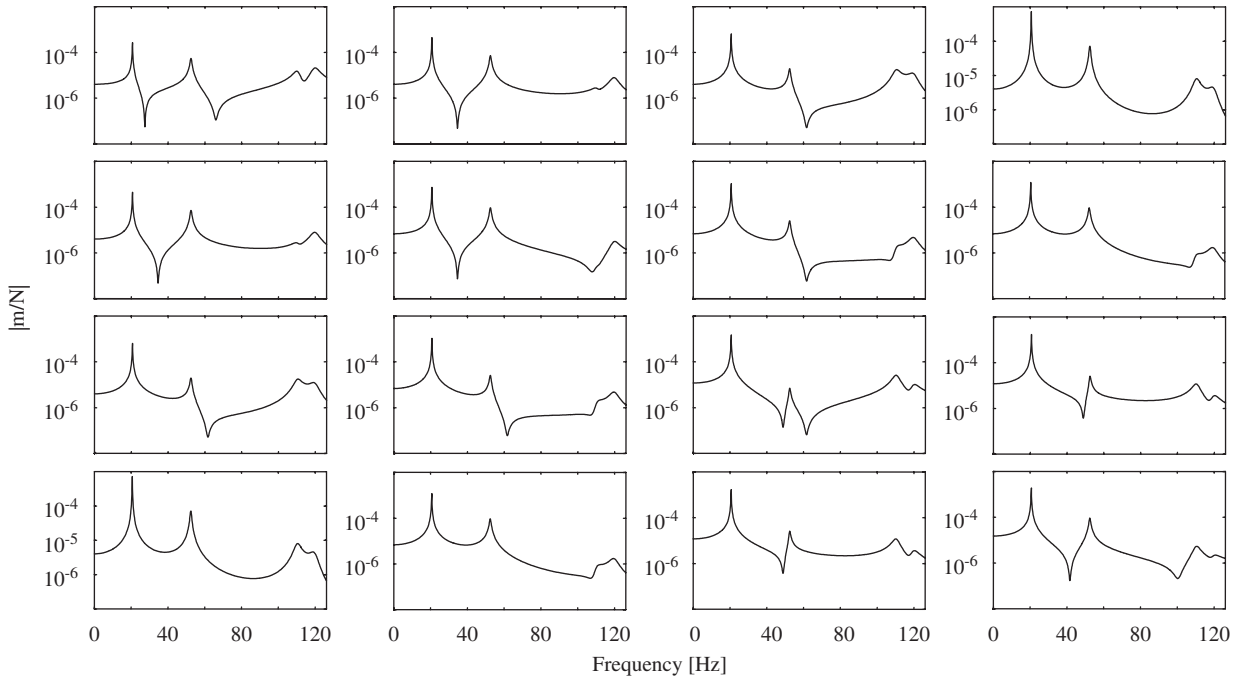

Fig. 11. Spatial plot of the frequency response function matrix for the 4 degrees of freedom original model.

range in which $\mathbf{T}(\omega)$ is almost real, the transformation matrix can be approximated as follows:

$$\mathbf{T}(\omega) \approx \tilde{\mathbf{T}}(\omega) = \begin{bmatrix} \mathbf{I} \\ -\left(-\omega^2\mathbf{M}_{\mathrm{uu}} + \mathbf{K}_{\mathrm{uu}}\right)^{-1}\left(-\omega^2\mathbf{M}_{\mathrm{um}} + \mathbf{K}_{\mathrm{uu}}\right) \end{bmatrix}. \tag{26}$$

The new matrix $\tilde{\mathbf{T}}(\omega)$ in Eq. (26) can be considered as a real-valued, approximate transformation matrix. Using this matrix in Eq. (21) combined with Eq. (25), the damping matrices of the models of two different sizes can now be related as follows:

$$\tilde{\mathbf{T}}(\omega)^{\mathrm{T}}\mathbf{L}(\omega)\tilde{\mathbf{T}}(\omega) = \mathrm{Imag}\left(\mathbf{S}_{D_R}(\omega)\right). \tag{27}$$

The frequency range in which Eq. (27) is valid has to be decided by considering the eigenvalues of $\mathbf{S}_{D_{\mathrm{uu}}}(\omega)$. A numerical study to determine the frequency range in conjunction with the eigenvalues of $\mathbf{S}_{D_{\mathrm{uu}}}(\omega)$ is conducted in Section 3.2.

3. Errors related to dynamic stiffness matrix approach

3.1. Errors induced by the dynamic stiffness matrix approach itself

The dynamic stiffness matrix method is a frequency domain method; therefore can be applied only to linearly behaving systems. While implementing the dynamic stiffness matrix approach described in Eqs. (2) and (3), both heavily and lightly damped systems will potentially pose challenges. Generally, a system is considered lightly damped when the average modal damping ratio is smaller than 1%. The challenge in lightly damped systems stems from the fact that the method tries to find the spatial distribution of very small quantities, thus even very small measurement errors are manifested in inverting the FRF matrix as in Eq. (2). A detailed study of the effect of measurement errors and their effects on the estimation of damping matrices is the subject of the on-going work of the authors.

The difficulty in a highly damped system is that the useful frequency range of the experimental model becomes small as the approximation associated with Eq. (27) has more pronounced effect.

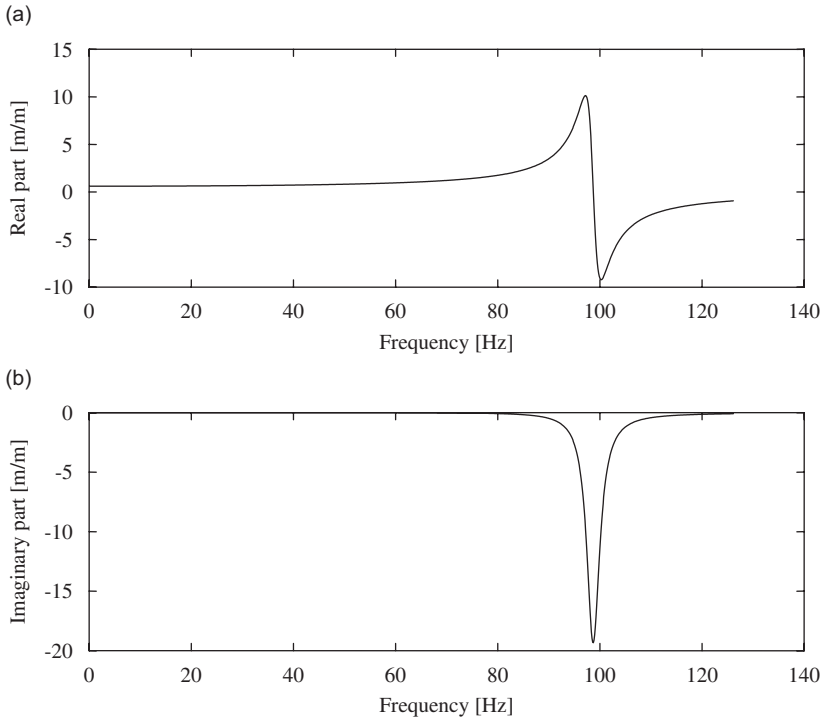

Fig. 12. Real and imaginary parts of the one of the elements of the transformation matrix $\mathbf{T}(\omega)$: (a) real part and (b) imaginary part.

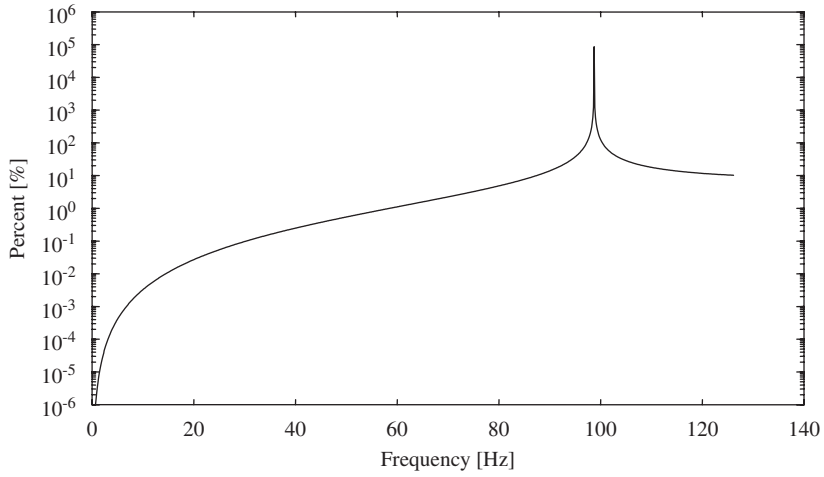

Fig. 13. Percent ratio of the real and imaginary parts of one of the elements of the transformation matrix $\mathbf{T}(\omega)$.

3.2. Error in relating experimental and analytical damping matrices

In order to understand the error associated with the expansion transformation in Eq. (27), which is $\tilde{\mathbf{T}}(\omega)^{\mathrm{T}}\mathbf{L}(\omega)\tilde{\mathbf{T}}(\omega) = \mathrm{Imag}\big(\mathbf{S}_{D_R}(\omega)\big)$, we consider three numerical examples. The first case is when a 4 dofs model is represented by a 2 dof experimental model, which was also used earlier in Section 2.3 as an example to study the frequency dependency of the transform. The second case is when a 10 dof model is represented by a 5 dof experimental model using its 2nd, 4th, 6th, 8th, and 10th degrees of freedom. The third case is when the same 10 dof model of the second case is represented by a 3 dof experimental model using its 1st, 5th, and 10th degrees of freedom.

First, the error norm to conduct the error analysis is defined as

$$\boldsymbol{\varepsilon}(\omega) = \mathrm{Imag}\left(\mathbf{S}_{D_R}(\omega)\right) - \tilde{\mathbf{T}}(\omega)^{\mathrm{T}}\mathbf{L}(\omega)\tilde{\mathbf{T}}(\omega), \tag{28}$$

where $\boldsymbol{\varepsilon}(\omega)$ is a matrix of size $M \times M$ which represents the error involved in Eq. (27) as a function of frequency. Then, the percent error matrix $\boldsymbol{\varepsilon}_p(\omega)$ is defined as follows.

$$\left(\boldsymbol{\varepsilon}_p(\omega)\right)_{ij} = \left|\frac{(\boldsymbol{\varepsilon}(\omega))_{ij}}{\mathrm{Imag}\left(\left(\mathbf{S}_{D_R}(\omega)\right)_{ij}\right)}\right| \times 100. \tag{29}$$

At each frequency, the maximum valued element in $\boldsymbol{\varepsilon}_p(\omega)$ is used to quantify the error associated with the transformation in Eq. (27).

We consider the first numerical case for when the system average modal damping ratio is 1.2%. The maximum value of the percent error matrix $\boldsymbol{\varepsilon}_p(\omega)$ for this particular damping level is plotted as a function of frequency in Fig. 14, showing that the maximum error is about 0.1% at a frequency of 63 Hz. This frequency is about 62% of the lowest eigenvalue of $\mathbf{S}_{D_{\mathrm{uu}}}(\omega)$, which is equal to 97 Hz. Looking at the same plot, we can also deduct that for the maximum value of the percent error to be equal to 1%, the ratio of the frequency to the lowest eigenvalue of $\mathbf{S}_{D_{\mathrm{uu}}}(\omega)$ should be 0.68.

Plots similar to Fig. 14 can be constructed at other levels of modal damping ratio. The error level will depend on the damping level as well as the reduction ratio of dofs. In order to study the effect of the reduction ratio, the second and third numerical cases are compared, which represent the same 10 degrees of freedom model by two experimental models of 5 and 3 dofs, respectively. Final results are presented in Figs. 15a and b, which show the frequency range for 0.1% and 1% error in terms of the ratio to the lowest eigenvalue of $\mathbf{S}_{D_{\mathrm{uu}}}(\omega)$. The comparisons are made for the range of 1–10% average modal damping ratio. As expected, the frequency limit for the transformation in Eq. (27) to be valid decreases as the damping level increases. The comparisons also show that the higher reduction ratio increases the error.

For example, Fig. 15a shows that the limiting frequency for an experimental model, in which Eq. (27) is valid within 0.1% error, is about 0.65 times the lowest eigenvalue of $\mathbf{S}_{D_{\mathrm{uu}}}(\omega)$. This is for the case when the average damping ratio is 1%. The limiting frequency is 0.45 times the lowest eigenvalue of $\mathbf{S}_{D_{\mathrm{uu}}}(\omega)$, if the system damping ratio level is about 10%. If the desired error level is 1%, Fig. 15b can be used in a similar way.

4. Expanding experimental damping matrix for hybrid modeling

Enabling the analytical–experimental hybrid modeling was the original motivation in developing the DSM-based damping identification method [23]. The idea is to build a simulation model of a dynamic system

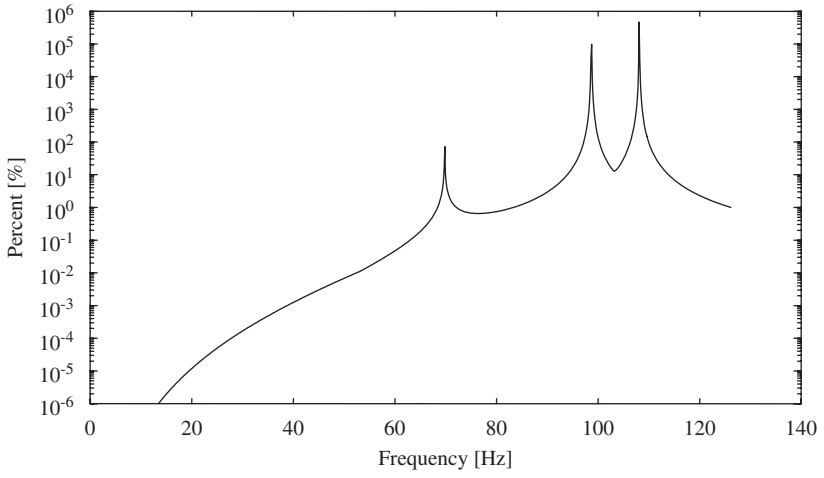

Fig. 14. Maximum percent error plot for Eq. (27).

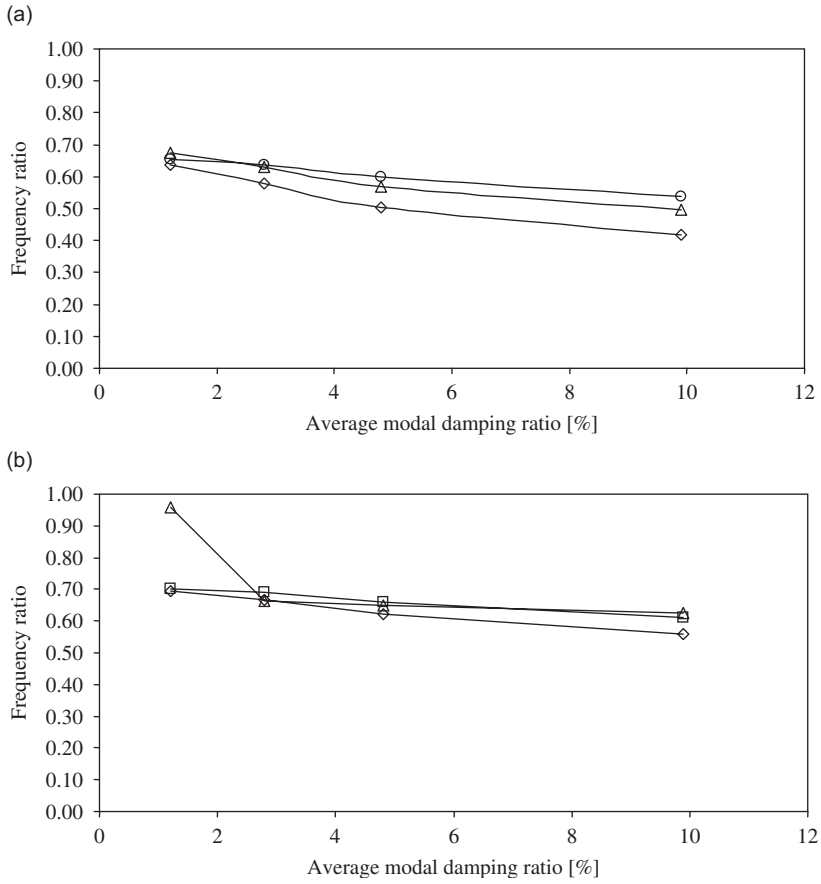

Fig. 15. Frequency ratio plot for different levels of error in Eq. (27): —◇—, Original Model: 4 degrees of freedom (1st,…,4th)/Experimental Model: 2 degrees of freedom (2nd and 4th); —△—, Original Model: 10 degrees of freedom (1st,…,10th)/Experimental Model: 5 degrees of freedom (2nd, 4th, 6th, 8th, 10th); —○—, Original Model: 10 degrees of freedom (1st,…,10th)/Experimental Model: 3 degrees of freedom (1st, 5th, 10th): (a) 0.1% error level; (b) 1% error level.

by combining analytically formulated mass and stiffness matrices with an experimentally identified damping matrix. The approach makes a perfect sense because the damping matrix cannot be formulated analytically like the mass and stiffness matrices. However, the damping matrix obtained from the DSM approach is much smaller than that of the analytical model in general; therefore the matrix should be expanded to the size of the analytical model. Two expansion methods are presented in Sections 4.1 and 4.2.

4.1. Method 1: expansion of damping matrix based on the transformation equation

4.1.1. Development of the method

Eq. (27) that relates the analytic damping matrix $\mathbf{L}(\omega)$ to the experimental damping matrix $\mathrm{Imag}(\mathbf{S}_{D_R}(\omega))$ can be used to expand the experimental damping matrix.

Because $\mathbf{L}(\omega)$ is a general function of frequency, Eq. (27) provides a new matrix relationship, thus a distinct set of linear equations, at each frequency point. However, because $\mathbf{L}(\omega)$ is a much bigger matrix than $\mathbf{S}_{D_R}(\omega)$, the number of unknowns to be found (N^2 at each frequency) far exceeds the number of equations available (M^2 at each frequency). The number of unknowns can be reduced substantially by assuming the form of the frequency dependency of $\mathbf{L}(\omega)$ as follows:

$$\mathbf{L}(\omega) = \sum_{i=1}^{S} f_i(\omega)\mathbf{C}_i, \tag{30}$$

where $f_i(\omega)$ is the ith frequency function, S is the number of frequency functions, $\mathbf{C}_i$ is the ith coefficient matrix.

Substituting Eq. (30) into Eq. (27):

$$\tilde{\mathbf{T}}(\omega)^{\mathrm{T}} \sum_{i=1}^{S} f_i(\omega)\mathbf{C}_i\tilde{\mathbf{T}}(\omega) = \mathrm{Imag}\big(\mathbf{S}_{D_R}(\omega)\big). \tag{31}$$

At each frequency, Eq. (31) provides M^2 linear equations of $\mathbf{C}_i$ in the following form:

$$\begin{aligned} &u_{j\times k}\big((\mathbf{C}_1)_{11},(\mathbf{C}_1)_{12},\ldots,(\mathbf{C}_1)_{NN},\ldots,(\mathbf{C}_2)_{NN},\ldots(\mathbf{C}_S)_{NN},\omega\big) = \mathrm{Imag}\Big(\big(\mathbf{S}_{D_R}(\omega)\big)_{jk}\Big),\\ &j = 1\ldots M \quad \text{and} \quad k = 1\ldots M, \end{aligned} \tag{32}$$

where u_n is the nth function with individual elements of coefficient matrices $\mathbf{C}_i$'s and frequency ω as independent variables. Unknown parameters in Eq. (32) are the elements of coefficient matrices $\mathbf{C}_i$'s. Therefore, the number of unknowns is $S\times N\times N$ where S is the number of frequency functions used in Eqs. (30) and (31). Eq. (32) can be set up at as many frequency points as necessary to have enough number of equations. If the number of equations exceeds the number of unknowns, the problem becomes over-determined and can be solved by a linear regression method.

For instance, if we assume a second-order polynomial type frequency distribution for the damping matrix, Eq. (30) reduces to

$$\mathbf{L}(\omega) = \mathbf{C}_1 + \omega\mathbf{C}_2 + \omega^{\mathbf{2}}\mathbf{C}_3, \tag{33}$$

where $f_1(\omega) = 1$, $f_2(\omega) = \omega$, and $f_3(\omega) = \omega^2$. $\mathbf{C}_1$, $\mathbf{C}_2$, and $\mathbf{C}_3$ are constant matrices that have to be found. Adding more polynomial terms in the form of $f_i(\omega) = \omega^i$, enables a more general representation of damping; however at the cost of increasing unknowns to be found.

4.1.2. Numerical example: viscously damped system

If the approach just discussed is applied assuming that the system is viscously damped, the damping function $f_1(\omega)$ will be equal to ω with $\mathbf{C}_1 = \mathbf{C}$ and $S = 1$. Therefore;

$$\mathbf{L}(\omega) = \omega\mathbf{C}. \tag{34}$$

In this case, Eq. (31) can be rewritten in a summation form as follows:

$$\tilde{\mathbf{T}}(\omega)^{\mathrm{T}}\mathbf{C}\tilde{\mathbf{T}}(\omega) = \frac{\mathrm{Imag}\big(\mathbf{S}_{D_R}(\omega)\big)}{\omega} \Rightarrow \cdots \sum_{k=1}^{N}\left(\sum_{j=1}^{N}\tilde{T}_{ji}C_{jk}\right)\tilde{T}_{ks} = \frac{\mathrm{Imag}\Big(S_{D_{R_{is}}}\Big)}{\omega}. \tag{35}$$

For one particular frequency, Eq. (35) can be expanded as

$$\begin{bmatrix} (\tilde{T}_{1i}\tilde{T}_{1s})_{\omega_1} & (\tilde{T}_{1i}\tilde{T}_{2s})_{\omega_1} & \cdots & (\tilde{T}_{1i}\tilde{T}_{Ns})_{\omega_1} & (\tilde{T}_{2i}\tilde{T}_{1s})_{\omega_1} & \cdots & (\tilde{T}_{Ni}\tilde{T}_{Ns})_{\omega_1} \end{bmatrix} \begin{Bmatrix} C_{11}\\ C_{12}\\ \vdots\\ C_{1N}\\ C_{2N}\\ \vdots\\ C_{NN} \end{Bmatrix} = \frac{\mathrm{Imag}\Big(S_{D_{R_{is}}}\Big)_{\omega_1}}{\omega_1}. \tag{36}$$

Right-hand side of Eq. (36), can also be written as a column vector; i.e.:

$$\begin{bmatrix} (\tilde{T}_{11}\tilde{T}_{11})_{\omega_1} & (\tilde{T}_{11}\tilde{T}_{21})_{\omega_1} & \cdots & (\tilde{T}_{11}\tilde{T}_{N1})_{\omega_1} & (\tilde{T}_{21}\tilde{T}_{11})_{\omega_1} & \cdots & (\tilde{T}_{N1}\tilde{T}_{N1})_{\omega_1} \\ (\tilde{T}_{11}\tilde{T}_{12})_{\omega_1} & (\tilde{T}_{11}\tilde{T}_{22})_{\omega_1} & \cdots & (\tilde{T}_{11}\tilde{T}_{N2})_{\omega_1} & (\tilde{T}_{21}\tilde{T}_{12})_{\omega_1} & \cdots & (\tilde{T}_{N1}\tilde{T}_{N2})_{\omega_1} \\ \vdots & \vdots & \ddots & \vdots & \vdots & \ddots & \vdots \\ (\tilde{T}_{11}\tilde{T}_{1M})_{\omega_1} & (\tilde{T}_{11}\tilde{T}_{2M})_{\omega_1} & \cdots & (\tilde{T}_{11}\tilde{T}_{NM})_{\omega_1} & (\tilde{T}_{21}\tilde{T}_{1M})_{\omega_1} & \cdots & (\tilde{T}_{N1}\tilde{T}_{NM})_{\omega_1} \\ (\tilde{T}_{12}\tilde{T}_{1M})_{\omega_1} & (\tilde{T}_{12}\tilde{T}_{2M})_{\omega_1} & \cdots & (\tilde{T}_{12}\tilde{T}_{NM})_{\omega_1} & (\tilde{T}_{22}T_{1M})_{\omega_1} & \cdots & (\tilde{T}_{N2}\tilde{T}_{NM})_{\omega_1} \\ \vdots & \vdots & \cdots & \vdots & \vdots & \ddots & \vdots \\ (\tilde{T}_{1M}\tilde{T}_{1M})_{\omega_1} & (\tilde{T}_{1M}\tilde{T}_{2M})_{\omega_1} & \cdots & (\tilde{T}_{1M}\tilde{T}_{NM})_{\omega_1} & (\tilde{T}_{2M}\tilde{T}_{1M})_{\omega_1} & \cdots & (\tilde{T}_{NM}\tilde{T}_{NM})_{\omega_1} \end{bmatrix} \begin{Bmatrix} C_{11} \\ C_{12} \\ \vdots \\ C_{1N} \\ C_{2N} \\ \vdots \\ C_{NN} \end{Bmatrix} \cdots = \frac{1}{\omega_1} \times \begin{Bmatrix} \mathrm{Imag}\left(S_{D_{R_{11}}}\right) \\ \mathrm{Imag}\left(S_{D_{R_{12}}}\right) \\ \vdots \\ \mathrm{Imag}\left(S_{D_{R_{1M}}}\right) \\ \mathrm{Imag}\left(S_{D_{R_{2M}}}\right) \\ \vdots \\ \mathrm{Imag}\left(S_{D_{R_{MM}}}\right) \end{Bmatrix}_{\omega_1} . \tag{37}$$

Eq. (37) can be written in a more compact form:

$$\mathbf{A}_{\omega_1} \begin{Bmatrix} C_{11} \\ C_{12} \\ \vdots \\ C_{1N} \\ C_{2N} \\ \vdots \\ C_{NN} \end{Bmatrix} = \frac{1}{\omega_1} \begin{Bmatrix} \mathrm{Imag}\left(S_{D_{R_{11}}}\right) \\ \mathrm{Imag}\left(S_{D_{R_{12}}}\right) \\ \vdots \\ \mathrm{Imag}\left(S_{D_{R_{1M}}}\right) \\ \mathrm{Imag}\left(S_{D_{R_{2M}}}\right) \\ \vdots \\ \mathrm{Imag}\left(S_{D_{R_{MM}}}\right) \end{Bmatrix}_{\omega_1} , \tag{38}$$

where $\mathbf{A}_{\omega_1}$ is the coefficient matrix shown in Eq. (37). Eq. (38) can be expanded by applying it at multiple frequencies (i.e. $\omega = \omega_1 \cdots \omega_k$):

$$\begin{bmatrix} \mathbf{A}_{\omega_1} \\ \vdots \\ \mathbf{A}_{\omega_k} \end{bmatrix} \begin{Bmatrix} C_{11} \\ C_{12} \\ \vdots \\ C_{1N} \\ C_{2N} \\ \vdots \\ C_{NN} \end{Bmatrix} = \begin{Bmatrix} \frac{1}{\omega_k} \begin{Bmatrix} \mathrm{Imag}\left(S_{D_{R_{11}}}\right) \\ \vdots \\ \mathrm{Imag}\left(S_{D_{R_{MM}}}\right) \end{Bmatrix}_{\omega_1} \\ \vdots \\ \frac{1}{\omega_k} \begin{Bmatrix} \mathrm{Imag}\left(S_{D_{R_{11}}}\right) \\ \vdots \\ \mathrm{Imag}\left(S_{D_{R_{MM}}}\right) \end{Bmatrix}_{\omega_k} \end{Bmatrix}. \tag{39}$$

Finally, the elements of the viscous damping matrix can be calculated from

$$\begin{Bmatrix} C_{11} \\ C_{12} \\ \vdots \\ C_{1N} \\ C_{2N} \\ \vdots \\ C_{NN} \end{Bmatrix} = \begin{bmatrix} \frac{1}{\omega_k} \begin{Bmatrix} \mathrm{Imag}\left(S_{D_{R_{11}}}\right) \\ \vdots \\ \mathrm{Imag}\left(S_{D_{R_{MM}}}\right) \end{Bmatrix}_{\omega_1} \\ \vdots \\ \frac{1}{\omega_k} \begin{Bmatrix} \mathrm{Imag}\left(S_{D_{R_{11}}}\right) \\ \vdots \\ \mathrm{Imag}\left(S_{D_{R_{MM}}}\right) \end{Bmatrix}_{\omega_k} \end{bmatrix} \begin{bmatrix} \mathbf{A}_{\omega_1} \\ \vdots \\ \mathbf{A}_{\omega_k} \end{bmatrix}^{+}. \tag{40}$$

Expansion of the experimental damping matrix $\mathrm{Imag}\left(S_{D_R}(\omega)\right)$ is conducted by solving Eq. (40). The right-hand side of this equation contains $\mathrm{Imag}\left(S_{D_R}(\omega)\right)$ and $\mathbf{A}_{\omega_1}$, which are expected to be available from experiment and analytical model, respectively. The unknown vector consists of the elements of the expanded viscous damping matrix $\mathbf{C}$, which is defined at the analytical model dof.

As a specific example, we consider a 10 degrees of freedom lumped parameter model shown in Fig. 16. The system parameters are $k = 2.5 \times 10^5$ N/m, $m = 1.0$ kg, and $c = 10.0$ N s/m. It is assumed that 2nd, 4th, 6th, 8$^{\text{th}}$, and 10th degrees of freedom are measured and they constitute the experimental model.

In order to decide the maximum frequency to use in the expansion procedure, the singular value plots of the measured frequency response function matrix shown in Fig. 17 can be used. From the singular value plots, the lowest eigenvalue of $\mathbf{S}_{D\mathrm{uu}}(\omega)$ is recognized as 115 Hz. The average modal damping ratio is estimated as about 2%. Based on Fig. 15a, the maximum frequency of the range is estimated as about 0.65 times of 115, or 74 Hz. This would limit the error associated with using Eq. (27) within 0.1%. Frequencies to implement Eq. (40) are chosen in this range.

The original damping matrix of the 10 degrees of freedom model is given in Table 1. The expansion process consists of computation of the elements of the expanded damping matrix using Eq. (40). The damping matrix obtained by expanding the 5×5 matrix corresponding to the 2nd, 4th, 6th, 8th, and 10th degrees of freedom, is given in Table 2. The expanded damping matrix is quite close to the original one, which demonstrates the validity of the proposed procedure to expand the experimental damping matrix.

In order to demonstrate the significance of using the proper frequency range, we apply the expansion procedure choosing frequency points from the range that includes the antiresonance point of the singular

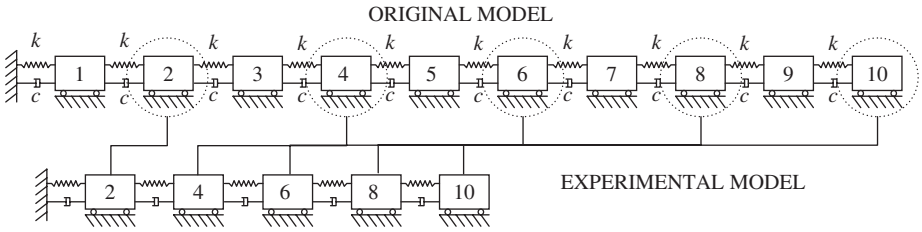

Fig. 16. Numerical example: 10 degree of freedom lumped parameter original model and 5 degrees of freedom experimental model.

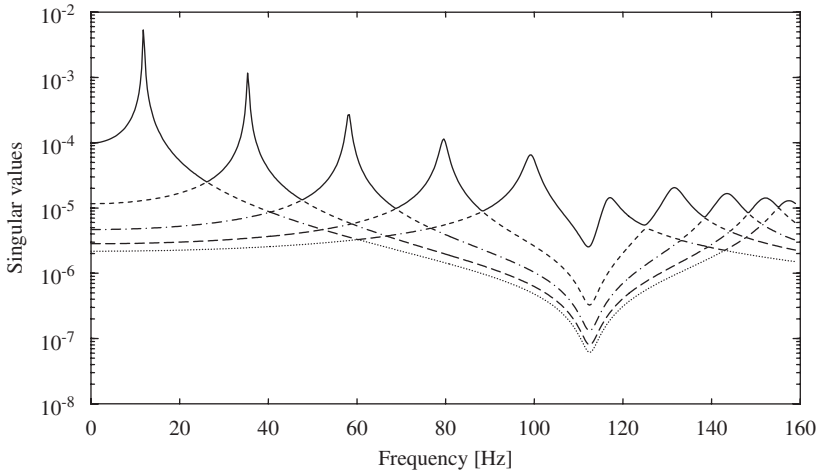

Fig. 17. Singular value plots for the 5 degrees of freedom experimental model: ——, largest singular value; - - - - - -, second largest singular value; –·–·–, third largest singular value; – – – –, fourth largest singular value; ·····, fifth largest singular value (lowest).

value plots. This introduces large errors in the basic transformation in Eq. (27). Expansion results are presented in Table 3, which show large errors as expected.

In order to test the expansion procedure for a nonproportional damping matrix, an additional case is considered where two of the damping coefficients for the 10 dof original model defined earlier are increased significantly. The damper that connects the fixed end to the 1st mass and the damper that connects the 6th and 7th masses are both increased by ten times. The new damping matrix, which is given in Table 4, represents a nonproportional system with two regions of localized damping.

Same 5×5 experimental model, which is composed of 2nd, 4th, 6th, 8th, and 10th dofs, is used to obtain the experimental DSM. Due to modified damping elements, the average modal damping ratio increases to about 3.8%. Considering this average damping ratio value and utilizing Fig. 15a, the maximum frequency of the range to be used in the matrix expansion process is estimated as about 0.5 times the lowest eigenvalue of $\mathbf{S}_{D_{\mathrm{uu}}}(\omega)$, which is identified earlier as 115 Hz from Fig. 17. The expanded damping matrix is given in Table 5. It successfully identifies the regions of high localized damping, however with reduced overall accuracy compared to the proportional damping case. This is probably caused by the increased error in the basic relationship Eq. (27), since overall damping level of the system is increased.

4.2. Method 2: simplified method of damping matrix expansion

In most practical applications, the analytical model is significantly larger than the experimental model. In such cases, the expansion method developed in Section 4.1 starts to become impractical as it requires solving for a huge number of unknowns. For example, if the analytical model has 1000 degrees of freedom—a modest size as a numerical model—and if the damping matrix is described by three constant matrices (see Eq. (33)), a total of 3,000,000 equations have to be solved. An alternative approach is expanding the identified

Table 1
Original viscous damping matrix of the 10 degrees of freedom lumped parameter model (units N s/m)

20	−10	0	0	0	0	0	0	0	0
−10	20	−10	0	0	0	0	0	0	0
0	−10	20	−10	0	0	0	0	0	0
0	0	−10	20	−10	0	0	0	0	0
0	0	0	−10	20	−10	0	0	0	0
0	0	0	0	−10	20	−10	0	0	0
0	0	0	0	0	−10	20	−10	0	0
0	0	0	0	0	0	−10	20	−10	0
0	0	0	0	0	0	0	−10	20	−10
0	0	0	0	0	0	0	0	−10	10

Table 2
Expanded viscous damping matrix of the 10 degrees of freedom lumped parameter model—1st case (units N s/m)

19.985	−9.992	0	0	0	0	0	0	0	0
−9.992	19.991	−9.992	−0.004	0	0	0	0	0	0
0	−9.992	19.985	−9.992	0	0	0	0	0	0
0	−0.004	−9.992	19.991	−9.992	−0.004	0	0	0	0
0	0	0	−9.992	19.985	−9.992	0	0	0	0
0	0	0	−0.004	−9.992	19.991	−9.992	−0.004	0	0
0	0	0	0	0	−9.992	19.985	−9.992	0	0.
0	0	0	0	0	−0.004	−9.992	19.991	−9.992	−0.004
0	0	0	0	0	0	0	−9.992	19.985	−9.992
0	0.	0	0	0	0	0	−0.004	−9.992	9.996

Table 3
Expanded viscous damping matrix of the 10 degrees of freedom lumped parameter model—2nd case (units N s/m)

0.167	−9.492	0	0	0	0	0	0	0	0
−9.492	352.83	−9.492	166.42	0	0	0	0	0	0
0	−9.492	0.167	−9.492	0	0	0	0	0	0
0	166.42	−9.492	352.83	−9.492	166.42	0	0	0	0
0	0	0	−9.492	0.167	−9.492	0	0	0	0
0	0	0	166.42	−9.492	352.83	−9.492	166.42	0	0
0	0	0	0	0	−9.492	0.167	−9.492	0	0
0	0	0	0	0	166.42	−9.492	352.83	−9.492	166.42
0	0	0	0	0	0	0	−9.492	0.167	−9.492
0	0	0	0	0	0	0	166.42	−9.492	176.42

Table 4
Original viscous damping matrix of the nonproportionally damped 10 degrees of freedom lumped parameter model (units N s/m)

110	−10	0	0	0	0	0	0	0	0
−10	20	−10	0	0	0	0	0	0	0
0	−10	20	−10	0	0	0	0	0	0
0	0	−10	20	−10	0	0	0	0	0
0	0	0	−10	20	−10	0	0	0	0
0	0	0	0	−10	110	−100	0	0	0
0	0	0	0	0	−100	110	−10	0	0
0	0	0	0	0	0	−10	20	−10	0
0	0	0	0	0	0	0	−10	20	−10
0	0	0	0	0	0	0	0	−10	10

Table 5
Expanded viscous damping matrix of the nonproportionally damped 10 degrees of freedom lumped parameter model (units N s/m)—1st case (units N s/m)

93.755	−8.473	6.781	1.332	−6.781	−1.813	9.589	−2.825	0	4.778
−8.473	17.981	−7.141	−0.003	−0.481	0.000	−4.638	0	1.953	0.000
6.781	−7.141	13.210	−13.701	6.781	6.931	−9.589	5.51	0	−6.731
1.332	−0.003	−13.701	19.995	−6.289	−0.003	17.078	0.000	−3.174	0
−6.781	−0.481	6.781	−6.289	13.210	−37.710	9.589	−19.413	0.000	9.905
−1.813	0	6.931	−0.003	−37.710	111.181	−74.201	−0.462	−6.335	0
9.589	−4.638	−9.589	17.078	9.589	−74.201	100.535	−9.189	0	−3.570
−2.825	0	5.510	0.000	−19.413	−0.462	−9.189	17.981	−6.425	−0.003
0	1.953	0	−3.174	0	−6.335	0	−6.425	19.990	−9.995
4.778	0	−6.731	0	9.905	0	−3.570	−0.003	−9.995	9.997

experimental damping matrix to the size of the analytical model, simply by embedding zero elements to the experimental damping matrix.

4.2.1. Development of the method

The DSM of an N degree of freedom model can be written in an expanded form to show measured and unmeasured components as follows (recall Eq. (12)):

$$\mathbf{S}_D(\omega) = \begin{bmatrix} -\omega^2\mathbf{M}_{\mathrm{mm}} + \mathrm{j}\mathbf{L}_{\mathrm{mm}} + \mathbf{K}_{\mathrm{mm}} & -\omega^2\mathbf{M}_{\mathrm{mu}} + \mathrm{j}\mathbf{L}_{\mathrm{mu}} + \mathbf{K}_{\mathrm{mu}} \\ -\omega^2\mathbf{M}_{\mathrm{um}} + \mathrm{j}\mathbf{L}_{\mathrm{um}} + \mathbf{K}_{\mathrm{um}} & -\omega^2\mathbf{M}_{\mathrm{uu}} + \mathrm{j}\mathbf{L}_{\mathrm{uu}} + \mathbf{K}_{\mathrm{uu}} \end{bmatrix}, \tag{41}$$

where subscript m and u indicates measured and unmeasured degrees of freedom. For the hybrid modeling, all the mass and stiffness matrices are assumed available. The damping matrix terms $\mathbf{L}_{\mathrm{mm}}$, $\mathbf{L}_{\mathrm{mu}}$, $\mathbf{L}_{\mathrm{um}}$, $\mathbf{L}_{\mathrm{uu}}$ are obtained from the damping matrix $\mathbf{L}_h(\omega)$, which is constructed by padding zeros to the experimental damping matrix $\mathrm{Imag}\big(\mathbf{S}_{D_R}(\omega)\big)$ at the unmeasured dofs, i.e.:

$$\mathbf{L}_h(\omega) = \begin{bmatrix} \mathrm{Imag}\big(\mathbf{S}_{D_R}(\omega)_{\mathrm{test}}\big) & \mathbf{0}_{\mathrm{mu}} \\ \mathbf{0}_{\mathrm{um}} & \mathbf{0}_{\mathrm{uu}} \end{bmatrix}, \tag{42}$$

where $\mathbf{0}$'s are zero matrices. The expansion defined in Eq. (42) implies that experimentally identified damping effect is distributed only at the measured dofs, which keeps the spatial information in a very approximated sense.

Now, combining the mass and stiffness matrices $\mathbf{M}$ and $\mathbf{K}$ from the analytical model and the expanded damping matrix $\mathbf{L}_h(\omega)$, the hybrid equation of motion is obtained as follows:

$$(-\omega^2\mathbf{M} + \mathrm{j}\mathbf{L}_h(\omega) + \mathbf{K})\mathbf{X}(\omega) = \mathbf{F}(\omega). \tag{43}$$

4.3. Numerical example

The validity of the proposed approach is demonstrated by using the same 10 dof lumped parameter model shown in Fig. 16, which was also used as the numerical example for the first expansion method. Same system parameters are used, which are $k = 2.5 \times 10^5$ N/m, $m = 1.0$ kg, and $c = 10.0$ N s/m. The experimental model is also composed of five of the dofs of the original model, which are 2nd, 4th, 6th, 8th, and 10th dofs.

The 5×5 damping matrix expanded by applying Eq. (42) is combined with the original 10×10 mass and stiffness matrices to make the hybrid model. The validity of the approach can be seen by comparing the frequency response functions obtained by solving the equations of motion of the original 10 dof model and the hybrid 10 dof model (see Figs. 18 and 19, respectively). At the measured dofs, the hybrid model accurately reproduces the original frequency response functions in the entire frequency range, as seen in the spatial plot for the measured portion of the FRF matrix $\mathbf{H}_{\mathrm{mm}}(\omega)$ (Fig. 18). Hybrid frequency response functions calculated at the unmeasured dof are accurate in the low-frequency range; however start to show large errors

around the lowest eigenvalue of $\mathbf{S}_{D_{uu}}(\omega)$, as can be seen in the spatial plot of the unmeasured portion of the FRF matrix $\mathbf{H}_{uu}(\omega)$ (Fig. 19).

This simple numerical example shows that if the hybrid model is used within the frequency range, for which Eq. (27) is valid, the model provides accurate results at all dofs. Even in the frequency range beyond the limit, the hybrid model provides accurate results, however, only for the FRFs at the measured dofs. Therefore, the valid frequency range for the hybrid model can be kept as same as the range of the experimental FRFs, only if the experimental model contains all the dofs at which we would like accurate synthesis of frequency response functions. Nevertheless, the method provides a very simple yet practical approach to expand the experimentally identified damping matrix to construct hybrid models.

5. Conclusion

Application of the DSM-based damping matrix identification method is discussed in this paper. This method offers several distinct advantages over other damping matrix identification methodologies that use the inherent assumption of proportional damping. Firstly, the damping matrix is obtained directly from experimental frequency response functions, which eliminates the need for experimental modal analysis to extract modal parameters. Secondly, the method offers a more accurate spatial distribution of the damping in the system because it does not use any assumption on the spatial distribution of damping as in the case of identifying damping by assuming proportional damping. Thirdly, the method finds the damping mechanism in a frequency-dependent form, which enables to identify damping mechanisms other than viscous damping.

The major contribution of this paper to the DSM-based methodology is to provide theoretical backgrounds to develop a method to expand the measured damping matrix to the size of the analytical model of significantly larger size. The motivation of the DSM-based method proposed by Lee and Kim [23] was to enable hybrid modeling by combining an experimentally obtained damping matrix with analytically formulated mass and stiffness matrices. In this paper, the errors associated with the identification method and the problems associated with expansion of the experimental matrix are studied with numerical examples. A method is established to estimate the frequency limit in

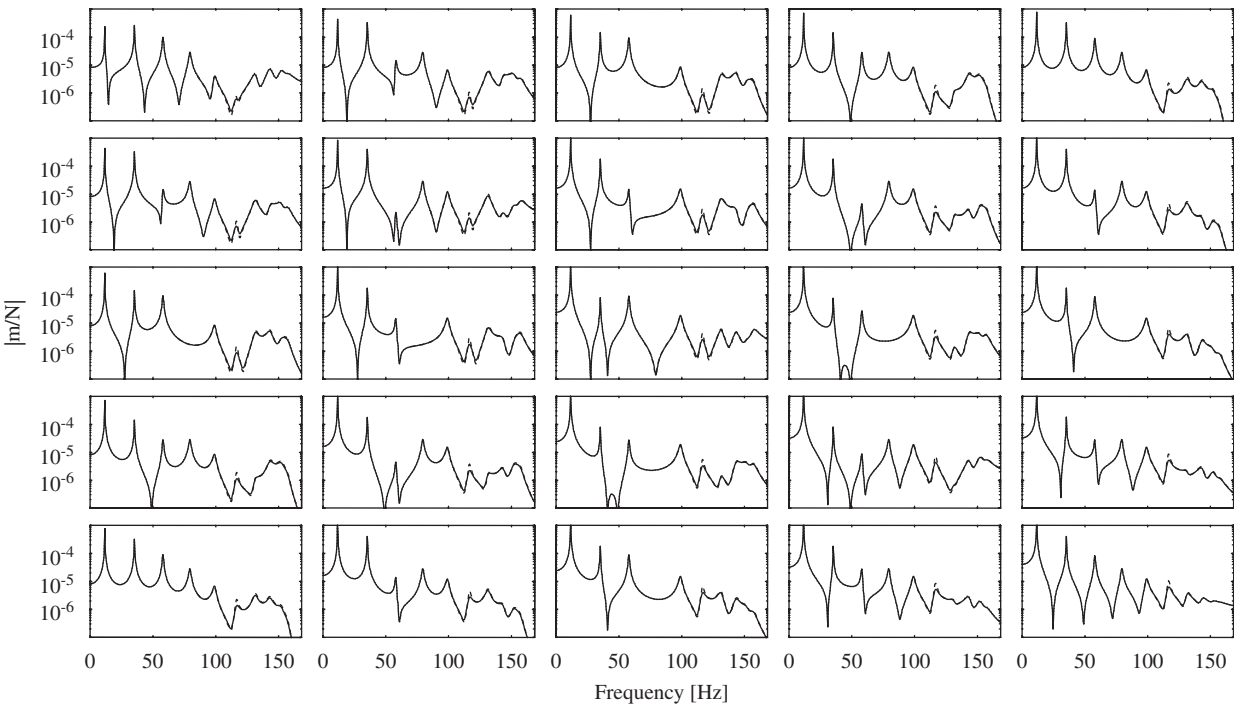

Fig. 18. Spatial plot of the measured portion of the frequency response function matrix $\mathbf{H}_{mm}(\omega)$: ——, original model; ------, hybrid model.

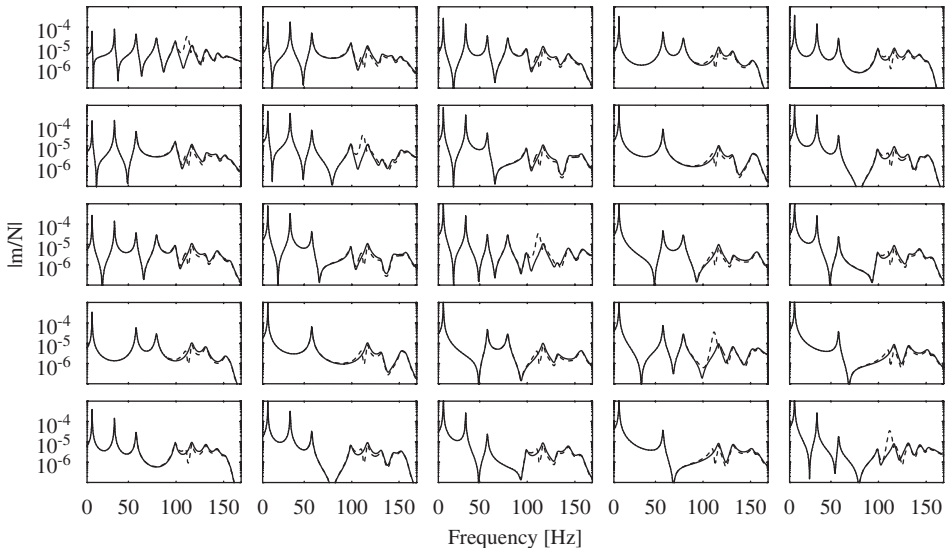

Fig. 19. Spatial plots of the unmeasured portion of the frequency response function matrix $\mathbf{H}_{uu}(\omega)$: ——, original model; ------, hybrid model.

which the damping matrix obtained from the DSM approach is valid. This method will serve as a useful guideline for effective use of the DSM-based damping identification approach as well as general experimental modeling.

Two approaches to expand the experimentally formulated damping matrix to the size of the analytic model are developed and discussed in detail. In the first approach, the experimental matrix is expanded by solving simultaneous equations derived from the transformation equation relating the experimental and analytical damping matrices. The second approach expands the experimental matrix by padding zeros to the elements of the matrix corresponding to the dofs that are not measured, which makes it a much simpler way compared to the first one. Also, the latter will be a more practical approach when the number of dofs of the system becomes large. Validity of both methods have been demonstrated with simple numerical examples. Further investigation and development of these methods are a part of authors' ongoing research work, which includes the cases of large model reduction/expansion, localized nonproportional damping, and nonviscous damping.

Appendix A. Reduced matrix representation of experimental dynamic stiffness matrix

The second part of Eq. (12) that relates the response and force vectors $\mathbf{X}(\omega)$ and $\mathbf{F}(\omega)$ is

$$\mathbf{S}_{D\mathrm{um}}(\omega)\mathbf{X}_m(\omega) + \mathbf{S}_{D\mathrm{uu}}(\omega)\mathbf{X}_u(\omega) = \mathbf{0}. \tag{A.1}$$

Therefore,

$$\mathbf{X}_u(\omega) = -\mathbf{S}_{D\mathrm{uu}}(\omega)^{-1}\mathbf{S}_{D\mathrm{um}}(\omega)\mathbf{X}_m(\omega) = \mathbf{R}_{\mathrm{um}}(\omega)\mathbf{X}_m(\omega), \tag{A.2}$$

where $\mathbf{R}_{\mathrm{um}}(\omega) = -\mathbf{S}_{D\mathrm{uu}}(\omega)^{-1}\mathbf{S}_{D\mathrm{um}}(\omega)$.

The response vector $\mathbf{X}(\omega)$ of the full size model and the measured response vector $\mathbf{X}_m(\omega)$ are related as follows:

$$\mathbf{X}(\omega) = \begin{Bmatrix} \mathbf{X}_m(\omega) \\ \mathbf{X}_u(\omega) \end{Bmatrix} = \begin{Bmatrix} \mathbf{X}_m(\omega) \\ \mathbf{R}_{\mathrm{um}}(\omega)\mathbf{X}_m(\omega) \end{Bmatrix} = \begin{bmatrix} \mathbf{I} \\ \mathbf{R}_{\mathrm{um}}(\omega) \end{bmatrix} \mathbf{X}_m(\omega) = \mathbf{T}(\omega)\mathbf{X}_m(\omega), \tag{A.3}$$

where $\mathbf{T}(\omega)$ is the transformation matrix and defined as follows:

$$\mathbf{T}(\omega) = \begin{bmatrix} \mathbf{I} \\ \mathbf{R}_{\mathrm{um}}(\omega) \end{bmatrix} = \begin{bmatrix} \mathbf{I} \\ -\mathbf{S}_{D\mathrm{uu}}(\omega)^{-1}\mathbf{S}_{D\mathrm{um}}(\omega) \end{bmatrix}. \tag{A.4}$$

The harmonic equation of motion of the experiment, based on the full size model is

$$\mathbf{S}_D(\omega)\mathbf{X}(\omega) = (-\omega^2\mathbf{M} + \mathrm{j}\mathbf{L}(\omega) + \mathbf{K})\mathbf{X}(\omega) = \begin{Bmatrix} \mathbf{F}_m(\omega) \\ \mathbf{0} \end{Bmatrix}. \tag{A.5}$$

Substituting Eq. (A.3) into Eq. (A.5),

$$(-\omega^2\mathbf{M} + \mathrm{j}\mathbf{L}(\omega) + \mathbf{K})\mathbf{T}(\omega)\mathbf{X}_m(\omega) = \begin{Bmatrix} \mathbf{F}_m(\omega) \\ \mathbf{0} \end{Bmatrix}. \tag{A.6}$$

If a force vector is defined such that $\mathbf{F}_m(\omega)_i = \mathbf{1}_{mi}$, which has all components as zero but the component at ith row is 1, the response vector becomes the FRF vector. Applying such a vector 1×1 to all measured dofs (i.e. $\mathrm{i} = 1 \ldots M$) and combining the results, the following equation is obtained:

$$(-\omega^2\mathbf{MT}(\omega) + \mathrm{j}\mathbf{L}(\omega)\mathbf{T}(\omega) + \mathbf{KT}(\omega))\mathbf{H}_{\mathrm{mm}}(\omega) = \begin{bmatrix} \mathbf{I}_{\mathrm{mm}} \\ \mathbf{0}_{\mathrm{um}} \end{bmatrix}. \tag{A.7}$$

Pre-multiply both sides of Eq. (A.7) by $\mathbf{T}(\omega)^{\mathrm{T}}$,

$$(-\omega^2\mathbf{T}(\omega)^{\mathrm{T}}\mathbf{MT}(\omega) + \mathrm{j}\mathbf{T}(\omega)^{\mathrm{T}}\mathbf{L}(\omega)\mathbf{T}(\omega) + \mathbf{T}(\omega)^{\mathrm{T}}\mathbf{KT}(\omega))\mathbf{H}_{\mathrm{mm}}(\omega) = \ldots \mathbf{T}(\omega)^{\mathrm{T}} \begin{bmatrix} \mathbf{I}_{\mathrm{mm}} \\ \mathbf{0}_{\mathrm{um}} \end{bmatrix}. \tag{A.8}$$

Noting that

$$\mathbf{T}(\omega)^{\mathrm{T}} \begin{bmatrix} \mathbf{I}_{\mathrm{mm}} \\ \mathbf{0}_{\mathrm{um}} \end{bmatrix} = \begin{bmatrix} \mathbf{I}_{\mathrm{mm}} & \mathbf{R}_{\mathrm{mu}}(\omega) \end{bmatrix} \begin{bmatrix} \mathbf{I}_{\mathrm{mm}} \\ \mathbf{0}_{\mathrm{um}} \end{bmatrix} = \mathbf{I}_{\mathrm{mm}},$$

Eq. (A.8) is now reduced to

$$(-\omega^2\mathbf{T}(\omega)^{\mathrm{T}}\mathbf{MT}(\omega) + \mathrm{j}\mathbf{T}(\omega)^{\mathrm{T}}\mathbf{L}(\omega)\mathbf{T}(\omega) + \mathbf{T}(\omega)^{\mathrm{T}}\mathbf{KT}(\omega))\mathbf{H}_{\mathrm{mm}}(\omega) = \mathbf{I}_{\mathrm{mm}}. \tag{A.9}$$

By definition, the dynamic stiffness matrix is the inverse of the frequency response function matrix, therefore, from Eq. (A.9):

$$-\omega^2\mathbf{M}_{R_{\mathrm{mm}}}(\omega) + \mathrm{j}\mathbf{L}_{R_{\mathrm{mm}}}(\omega) + \mathbf{K}_{R_{\mathrm{mm}}}(\omega) = \cdots - \omega^2\mathbf{T}(\omega)^{\mathrm{T}}\mathbf{MT}(\omega) + \mathrm{j}\omega\mathbf{T}(\omega)^{\mathrm{T}}\mathbf{L}(\omega)\mathbf{T}(\omega) + \mathbf{T}(\omega)^{\mathrm{T}}\mathbf{KT}(\omega). \tag{A.10}$$

Now, the matrices of the reduced-size experimental and full-size analytical models are related as

$$\mathbf{M}_{R_{\mathrm{mm}}}(\omega) = \mathbf{T}(\omega)^{\mathrm{T}}\mathbf{MT}(\omega), \tag{A.11}$$

$$\mathbf{L}_{R_{\mathrm{mm}}}(\omega) = \mathbf{T}(\omega)^{\mathrm{T}}\mathbf{L}(\omega)\mathbf{T}(\omega), \tag{A.12}$$

$$\mathbf{K}_{R_{\mathrm{mm}}}(\omega) = \mathbf{T}(\omega)^{\mathrm{T}}\mathbf{KT}(\omega). \tag{A.13}$$

The dynamic stiffness matrix of the experimental model is

$$\mathbf{S}_{D_R}(\omega) = -\omega^2\mathbf{M}_{R_{\mathrm{mm}}}(\omega) + \mathrm{j}\omega\mathbf{C}_{R_{\mathrm{mm}}}(\omega) + \mathbf{K}_{R_{\mathrm{mm}}}(\omega). \tag{A.14}$$

References

[1] R.M. Christensen, *Theory of Viscoelasticity, An Introduction*, Academic Press, New York, 1971.
[2] R.S. Lakes, *Viscoelastic Solids*, CRC Press LLC, Boca Raton, 1999.
[3] E.J. Berger, Friction modeling for dynamic system simulation, *Applied Mechanics Reviews* 55 (6) (2002) 535–577.
[4] Z. Osinski (Ed.), *Damping of Vibrations*, A.A. Balkema, Rotterdam, Brookfield, 1998.
[5] A.D. Nashif, D.I.G. Jones, J.P. Henderson, *Vibration Damping*, Wiley Interscience, New York, 1985.
[6] D.I.G. Jones, *Handbook of Viscoelastic Vibration Damping*, Wiley, West Sussex, 2001.
[7] M. Link, Identification of physical system matrices using incomplete vibration test data, *Proceedings of the fourth International Modal Analysis Conference*, *Los Angeles,* CA, Vol. 1, 1986, pp. 386–393.

[8] M. Link, M. Weiland, J.M. Barragán, Direct physical matrix identification as compared to phase resonance testing: an assessment based on practical application, *Proceedings of the fifth International Modal Analysis Conference, London, England*, Vol. 1, 1987, pp. 804–811.
[9] Y.W. Luk, Identification of physical mass, stiffness and damping matrices using pseudo-inverse, *Proceedings of the fifth International Modal Analysis Conference, London, England*, Vol. 1, 1987, pp. 679–685.
[10] K. Shye, M. Richardson, Mass, stiffness, and damping matrix estimates from structural measurements, *Proceedings of the fifth International Modal Analysis Conference*, *London, England*, Vol. 1, 1987, pp. 756–761.
[11] N.G. Creamer, J.L. Junkins, Identification method for lightly damped structures, *Journal of Guidance* 11 (6) (1988) 571–576.
[12] W.F. Tsang, E. Rider, The technique of extraction of structural parameters from experimental forced vibration data, *Proceedings of the seventh International Modal Analysis Conference*, Vol. 2, 1989, pp. 1627–1633.
[13] J.L. Jensen, R. Brincker, A. Rytter, Identification of light damping in structures, *Proceedings of the Eighth International Modal Analysis Conference*, Kissimmee, FL, Vol. 2, 1990, pp. 1041–1047.
[14] D.F. Pilkey, D.J. Inman, An iterative approach to viscous damping matrix identification, *Proceedings of the 15th International Modal Analysis Conference*, *Orlando, FL,* Vol. 1, 1997, pp. 104–110.
[15] D.F. Pilkey, P. Gyuhae, D.J. Inman, Damping matrix identification and experimental verification, *Smart Structures and Materials, SPIE Conference on Passive Damping and Isolation, Newport Beach, California*, 1999, pp. 350–357.
[16] S. Adhikari, J. Woodhouse, Towards identification of a general model of damping, *Proceedings of the 18th International Modal Analysis Conference*, San Antonio, TX, Vol. 1, 2000, pp. 377-383.
[17] D.J. Henwood, Approximating the hysteretic damping matrix by a viscous matrix for modelling in the time domain, *Journal of Sound and Vibration* 254 (3) (2002) 575–593.
[18] S.R. Ibrahim, W. D'ambrogio, P. Salvini, A. Sestieri, Direct updating of nonconservative finite element models using measured input-output, *Proceedings of the 10th International Modal Analysis Conference*, Vol. 1, 1992, pp. 202–210.
[19] S. Lammens, M. Brughmans, J. Leuridan, P. Sas, Application of a FRF based model updating technique for the validation of finite element models of components of the automotive industry, *Proceedings of the 1995 Noise and Vibration Conference, SAE International*, Traverse City, Michigan, USA, Vol. 1, 1995, pp. 103–115.
[20] S.Y. Chen, M.S. Ju, Y.G. Tsuei, Stiffness and damping matrices from frequency response functions, *ASME Journal of Vibration and Acoustics* 118 (1996) 78–82.
[21] M. Dalenbring, Damping function estimation based on measured vibration frequency responses and finite-element displacement modes, *Mechanical Systems and Signal Processing* 13 (1999) 547–569.
[22] J.H. Lee, J. Kim, Identification of damping matrices from measured frequency response functions, *Journal of Sound and Vibration* 240 (3) (2001) 545–565.
[23] J.H. Lee, J. Kim, Development and validation of a new experimental method to identify damping matrices of a dynamic system, *Journal of Sound and Vibration* 246 (3) (2001) 505–524.
[24] J.E. Hylok, Experimental Identification of Distributed Damping Matrices using the Dynamic Stiffness Matrix, Thesis (M.S.), University of Cincinnati, 2002.
[25] G.O. Ozgen, J. Kim, Further Developments in the dynamic stiffness Matrix (DSM) based direct damping identification method, *SAE Noise and Vibration Conference, Traverse City, MI*, 2005.
[26] G.O. Ozgen, J. Kim, Applications of the dynamic stiffness matrix (DSM) based direct damping identification method, *SAE Noise and Vibration Conference*, *Traverse City, MI,* 2005.
[27] J. O'Callahan, P. Avitable, R. Riemer, System equivalent reduction expansion process (SEREP), *Proceedings of the seventh International Modal Analysis Conference*, Vol. 1, 1989, pp. 29–37.
[28] J. O'Callahan, A procedure for an improved reduced system (IRS) model, *Proceedings of the seventh International Modal Analysis Conference*, Vol. 1, 1989, pp. 17–21.
[29] J. O'Callahan, Reduced model concepts, *Proceedings of the 18th International Modal Analysis Conference*, San Antonio, TX, USA, Vol. 2, 2000, pp. 1528–1536.
[30] M.I. Friswell, J.E. Mottershead, *Finite Element Model Updating in Structural Dynamics*, Kluwer Academic Publishers, Dordrecht, Netherlands, 1995.
[31] Y. Ye, Z. Qu, Iterative methods for dynamic condensation of structural matrices, *Proceedings of the 18th International Modal Analysis Conference*, San Antonio, TX, USA, Vol. 2, 2000, pp. 1776–1782.
[32] M. Paz, Dynamic condensation, *AIAA Journal* 22 (5) (1984) 724–727.
[33] A. Berman, Identification of structural dynamic models—theoretical and practical bounds, *System AIAA/ASME/ASCE/AHS 25th Structures*, *Structural Dynamics & Materials Conference*, San Antonio, TX, USA, Vol. 2, 1984, pp. 123–129.
[34] A. Berman, Validity of improved mathematical models, a commentary, *Proceedings of the 16th International Modal Analysis Conference*, Palm Springs, California, USA, Vol. 1, 1998, pp. 681–691.
[35] A. Berman, Inherently incomplete finite element model and its effects on model updating, *AIAA Journal* 38 (11) (2000) 2142–2146.
[36] S. Lammens, M. Brughmans, J. Leurian, P. Sas, Updating of dynamic finite element models based on experimental receptances and the reduced analytical dynamic stiffness matrix, *Proceedings of the 1995 Noise and Vibration Conference, SAE International*, Santa Barbara, California, USA, Vol. 1, 1995, pp. 117–126.
[37] N. Bouhaddi, S. Cogan, R. Fillod, Dynamic substructuring by Guyan condensation selection of the master dof, *Proceedings of the 10th International Modal Analysis Conference*, Vol. 1, 1992, pp. 328–333.